Journal of Urban Mobility 9 (2026) 100209

Contents lists available at ScienceDirect

Journal of Urban Mobility

journal homepage: www.elsevier.com/locate/urbmob

Vulnerability assessment of urban road networks under extreme weather events

Francesco Guglielmi *, Pietro Mariano, Pierluigi Coppola

Department of Mechanical Engineering, Politecnico di Milano, via Giuseppe La Masa 1, Milano, 20156, MI, Italy

ARTICLE INFO

Keywords:
Flood risk
Multi-scenario analysis
Demand heterogeneity
Traffic assignment
Resilience

ABSTRACT

The increasing occurrence of extreme weather events poses significant challenges to urban road transport systems, as spatially diffused disruptions (e.g., flooding) can trigger congestion spillovers and network-wide performance losses. This study proposes a multi-scenario, demand-segmented framework to assess flood-induced transport vulnerability and applies it to the private road network of the Milan metropolitan area. Flood hazard maps are used in combination with a static traffic assignment model to simulate performance degradation under multiple flood scenarios. A composite link-level vulnerability indicator is introduced, combining local congestion effects with systemic relevance measures derived from network-wide travel time changes, and is applied across distinct demand segments. Results show that vulnerabilities concentrate along ring-road systems and their access corridors, with inter-ring and external trips experiencing the greatest impacts, while internal trips are mainly affected by localized congestion. The findings demonstrate that flood-induced transport vulnerability is strongly shaped by demand patterns, network structure and exposure to risk. The proposed framework supports policy-oriented identification of critical road links and targeted preparedness strategies, and it is transferable to other metropolitan areas with comparable urban forms and flood exposure.

1. Introduction

The increasing frequency and intensity of extreme weather events have posed significant challenges to the functioning of transport systems worldwide. Among these, flooding stands out as one of the most recurrent and disruptive hazards, capable of severely impairing network performance and reducing accessibility. Understanding and quantifying how transportation systems withstand flood-related disruptions is thus essential for pinpointing system vulnerabilities, and developing effective preparedness and mitigation strategies accordingly, with the ultimate objective of enhancing resilience (ITF 2016).

In transport planning, the concepts of resilience and vulnerability have become central to the analysis of transport systems exposed to extreme weather events. Resilience is commonly defined as the ability of a transport system to absorb disturbances, adapt to changing conditions, and recover while maintaining acceptable levels of service. According to the International Transport Forum (ITF), resilience is a measure of the system's ability not only to absorb shocks but also to adapt and transform to future conditions (ITF 2024), emphasizing the role of proactive planning in managing risks and uncertainties, such as those related to climate change and disruptive technologies (Coppola and Esztergár-Kiss, 2019). Early work framed resilience as a multidimensional property related to the system's ability to reduce the likelihood and consequences of failures and to shorten recovery times, highlighting key dimensions such as robustness, redundancy, resourcefulness, and rapidity (Bruneau et al., 2003). From a planning perspective, resilience has also been interpreted as the outcome of mitigation and adaptation strategies, highlighting the relevance of vulnerability assessment for policy making (McDaniels et al., 2008). More recent studies emphasize the need for integrated assessment frameworks that explicitly account for interactions between infrastructure, demand, and operations, moving towards a systemic interpretation of transport resilience as the joint influence between network topology, operational conditions, user behaviour, and institutional preparedness (Bešinović, 2020; Gonçalves and Ribeiro, 2020).

Another key concept is vulnerability, that is the degree of performance loss experienced by the system when exposed to a disruptive event (Bruneau et al., 2003; Gonçalves and Ribeiro, 2020; Berdica, 2002). Thus, it can be interpreted as the dual concept of robustness, which is a core component of resilience (McDaniels et al., 2008). As

* Corresponding author.
E-mail address: francesco.guglielmi@polimi.it (F. Guglielmi).

https://doi.org/10.1016/j.urbmob.2026.100209
Received 10 November 2025; Received in revised form 13 March 2026; Accepted 13 March 2026
Available online 27 March 2026

such, a highly vulnerable transport system is one that exhibits low robustness, i.e., a high susceptibility to functional degradation after a shock. Henceforth, while resilience encompasses recovery and adaptive capacity over time, vulnerability primarily focuses on the immediate performance loss following a disruption. Accordingly, the present study focuses primarily on vulnerability, by assessing the immediate and short-term performance degradation rather than on dynamic recovery processes from disruption. In the context of transport planning and policy making, vulnerability analyses provide a quantitative basis to identify critical components whose failure would negatively affect the system. A growing body of research has employed both topological and simulation-based approaches to capture these effects, progressively integrating hazard modelling and demand–supply dynamics. The use of transportation modelling and link-level vulnerability indicators is particularly relevant in the case of flooding, where performance degradation is not concentrated to one or few network links, but it is spatially distributed.

In dense metropolitan areas, even short-term inundation can lead to severe traffic congestion, accessibility loss, and cascading effects to other infrastructure systems. The city of Milan has historically been exposed to recurrent flooding events primarily associated with the Seveso and Lambro rivers. Over the past decades, these events have become increasingly frequent and disruptive, with direct impacts on road accessibility, safety, and mobility efficiency. Between 1976 and 2023, the Seveso River alone has flooded a total of 120 times (Comune di Milano), generating disruptive effects on both private and public transport systems. As climate change continues to intensify precipitation patterns, the potential impacts of flooding on the city's road transport system are expected to grow (Comune di Milano; Comune di Milano).

Despite Milan's recurrent exposure to flood events, the vulnerability of its urban road network has received limited attention in the literature. From a morphological and infrastructural perspective, Milan is representative of many large European metropolitan areas: it is in a predominantly flat and water-rich territory and has developed without major natural barriers, resulting in a concentric urban form structured around arterial ring roads and radial access corridors. This configuration, common to several European cities, makes Milan a particularly relevant case for investigating how spatially distributed flood hazards affect urban road network vulnerability and for deriving insights that are potentially transferable beyond the local context. Furthermore, existing vulnerability assessments often provide limited representations of flood-related impacts on urban mobility. Traffic demand is frequently treated in an aggregate manner, hazard uncertainty is commonly explored through a limited number of scenarios, and vulnerability metrics are typically designed to capture system-wide effects of isolated failures rather than link-level vulnerabilities arising from spatially distributed performance degradation, which is more consistent with the nature of urban flooding.

The present study addresses these limitations by analysing the systemic vulnerabilities of Milan's private road transport system to flood risks associated with the Seveso and Lambro rivers. To this end, a multi-scenario and demand-segmented assessment methodology is applied. The approach combines geospatial flood data developed by the Po River Basin Authority (ADBPO) with a traffic simulation model of private transport in Milan. For each flood scenario, the reduction in travel speed of affected road links is simulated, and the resulting network performance losses are evaluated. Simulation outcomes are then synthesised into a composite link vulnerability index that captures uncertainty across scenarios. Results disaggregation to specific demand segments allows for the identification of segment-specific critical road links across the urban area, enabling the design of mitigation and preparedness strategies that account for demand heterogeneity.

This paper is organised as follows: Section 2 reviews the recent literature on urban flood vulnerability assessment case studies, and on multi-scenario and demand segmentation-based approaches. Section 3 describes the proposed multi-scenario vulnerability assessment framework, while Section 4 describes the case study of application. Section 5 presents and discusses preliminary findings from flood scenarios simulation, whose result are quantitatively analysed and discussed in Section 6 via the application of the proposed vulnerability assessment methodology. Section 7 concludes with key insights and the policy implications for enhancing transport system robustness to flooding, methodological limitations and proposed research developments.

2. Literature review

Methodologies for assessing transport system vulnerability are commonly classified into topological and systemic approaches (Mattsson and Jenelius, 2015). Topological approaches focus on the structural properties of the network, using graph-theory indices such as betweenness centrality, node degree, or network efficiency to identify critical nodes or links whose failure would compromise connectivity and/or network performances (Mattsson and Jenelius, 2015, Jafino, Kwakkel, and Verbraeck, 2020). While computationally efficient and useful for preliminary screening or network comparison, these methods typically neglect demand-supply interactions, congestion effects, and behavioural responses. Systemic approaches, by contrast, explicitly model traffic flows, congestion dynamics, and user adaptation under disruption, allowing for a more comprehensive simulation of the disrupted system (Mattsson and Jenelius, 2015, Zhou, Wang, and Yang, 2019). For these reasons, systemic approaches are increasingly adopted in vulnerability assessments under hazardous events, as they enable a direct linkage between infrastructure damage and service degradation (Sun, Bocchini, and Davison, 2020). Although topological analyses remain valuable as low-cost tools for identifying potentially weak network elements (Almotahari and Yazici, 2020), systemic approaches that leverage traffic simulation models are better suited for multi-scenario vulnerability assessments, particularly when spatially distributed hazards must be considered (Jafino, Kwakkel, and Verbraeck, 2020). This distinction becomes particularly relevant in the case of flooding, where disruptions typically affect extended portions of the network through partial (or complete) performance degradation rather than isolated link failures. This makes vulnerability hard to infer from topology alone: localized flooding events can trigger traffic rerouting, congestion spillovers and network-wide effects that depend on the interaction between the impacted area, the magnitude of the impact, as well as transport supply and demand patterns. Consequently, flood vulnerability assessment increasingly relies on modelling frameworks that translate hazard data (e.g., extension, depth, return period) into link performance degradation or closure, and propagate impacts through traffic assignment models to quantify losses in travel time, accessibility, or generally, system performances (e.g., (Chen, Lu, Peng, and Ash, 2015, Shen and Kim, 2020, Pregnolato, Ford, Wilkinson, and Dawson, 2017, Pregnolato et al., 2016)).

However, a stream of academic work focuses on the identification of critical elements via empirical analysis or topological indices (e.g., betweenness centrality, network efficiency, connectivity, etc.). These methods are useful for pinpointing critical points in the network especially in the context of data scarcity (e.g., (Papilloud and Keiler, 2021, Loreti et al., 2022)). As previously discussed, for flooding assessment they face a key limitation: they typically treat disruptions as binary (i.e., a network link is either open or closed), neglect intensity of the event, and omit demand–supply interaction and congestion dynamics. As a result, they are not well suited to model the impact of hazards like flooding, where vulnerability is driven by how traffic redistributes across the network.

As such, a second stream in the literature integrates flood hazard data with transport models to simulate how link performance degradation impacts traffic. This includes approaches based on static assignment, simulation or hybrid approaches (e.g., (Chen, Lu, Peng, and Ash, 2015, Shen and Kim, 2020, Abdulla, Kiaghadi, Rifai, and Birgisson,

Table 1
Key contributions to the literature on flood vulnerability assessments.

Study	Year	Transport system	Location	Hazard data	Method / model	Multi-scenario (how / combined)	Demand heterogeneity?	Vulnerability indicator (level)
Abdulla et al. (Abdulla, Kiaghadi, Rifai, and Birgisson, 2020)	2020	Urban road	Houston, USA	Yes (mapping of spatiotemporal network exposed elements to floods from a hydraulic model)	SIS diffusion model with flood depth–speed reduction function	Yes, reported separately	Aggregate	Topological and connectivity metrics (network and link-level)
Borowska-Stefańska et al. (Borowska-Stefańska et al., 2025)	2024	Urban road	Łódź, Poland	Yes (discrete-depth hazard maps)	Accessibility-based network analysis (GIS) with flood depth–speed reduction function	Yes, reported separately	Aggregate	Accessibility loss (TAZ-level)
Borowska-Stefańska et al. (Borowska-Stefańska et al., 2024)	2025	Urban road	Łódź, Poland	Yes (discrete-depth hazard maps)	Microsimulation of a section of the network	No	Aggregate	Delay times, the number of vehicle holdups and queuing times (network level)
Chen et al. (Chen, Lu, Peng, and Ash, 2015)	2015	Urban road	Tampa Bay, USA	Yes (combination of predicted sea level rise and TAZ elevation)	Static assignment with reduced link capacity	Yes, arbitrary scenarios of link capacity reduction combined by probability of sea-level rise	Yes, different travel modes are considered	Accessibility loss (TAZ-level)
Dong et al. (Dong, Gao, Mostafavi, and Gao, 2022)	2022	Urban road	Harri County, USA	Yes (empirical data on traffic speed reduction caused by hurricane-induced flooding)	Topological (percolation theory)	Yes, time-variant scenarios	Aggregate	Network performance and robustness indices (network-level)
Dowds et al. (Dowds, Sentoff, Sullivan, and Aultman-Hall, 2017)	2017	Urban road	Chittenden County, USA	No flood data, but generic link removal	Static assignment	No	Yes	Network Robustness Index (network-level)
Lin et al. (Lin, Lu, Chen, and Brilakis, 2024)	2024	Urban road	London, UK	Yes (dynamic evolution of flooding)	Dynamic network analysis with demand data	Yes, time-variant scenarios	Aggregate	Time-variant vulnerability index (link-level)
Loreti et al. (Loreti et al., 2022)	2022	Urban road	Canton of Bern, Switzerland	Yes (spatio temporal hazard evolution maps)	Topological (perculation theory)	No	Aggregate	Topological and connectivity metrics (network level)
Marian et al. (Marian, Hijazi, Masad, and Abdel-Wahab, 2024)	2024	Urban road	Doha, Qatar	Yes (historical data)	Meso-scale simulation of critical subnetworks	Yes, reported separately	Aggregate	Both network-level and link-level vulnerability indices
Pagliara & Zingone (Pagliara and Zingone, 2023)	2023	Airport access	Milan, Italy	No, deterministic base and project scenarios with monetized flood damage savings	Cost-benefit analysis (CBA) with a transport demand model	Limited (only base and project scenario)	Aggregate	Financial and Economic indicators
Papilloud & Keiler (Papilloud and Keiler, 2021)	2021	Urban road	Canton of Bern, Switzerland	Yes (hazard maps for a total of 150 flood scenarios)	Comparison of accessibility-based and topological vulnerability indices	Yes, reported separately	Aggregate	Accessibility loss (TAZ-level)
Pregnolato et al. (Pregnolato et al., 2016)	2016	Urban road	Newcastle upon Tyne, UK	Yes (raster hazard maps from a hydrodynamic model)	Static assignment with flood depth–speed reduction function	Yes, reported separately	No	Total time of delay, person minute delay (network-level), weighted betweenness centrality (link-level)
Shen & Kim (Shen and Kim, 2020)	2020	Urban road	Honolulu, Hawaii	Yes (tidal flood maps from a simplified bathtub model and topography data)	Accessibility-based network analysis (GIS)	Yes, reported separately	Yes, different population strata are considered	Accessibility loss (TAZ-level)
Tsang & Scott (Tsang and Scott, 2020)	2020	Urban road	Calgary, Canada	Yes, multi-source estimation of a 100-year TR flood	Accessibility-based network analysis (GIS) with flood depth–speed reduction function	No	No	Accessibility to emergency services (TAZ-level)
This study	**2026**	**Urban road**	**Milan, Italy**	**Yes, flood hazard maps with assumed water depths**	**Static assignment with depth–speed reduction functions**	**Yes, combined into a single vulnerability metric**	**Yes, demand is segmented geographically**	**Segment-specific, systemic, and multi-scenario vulnerability indicator**

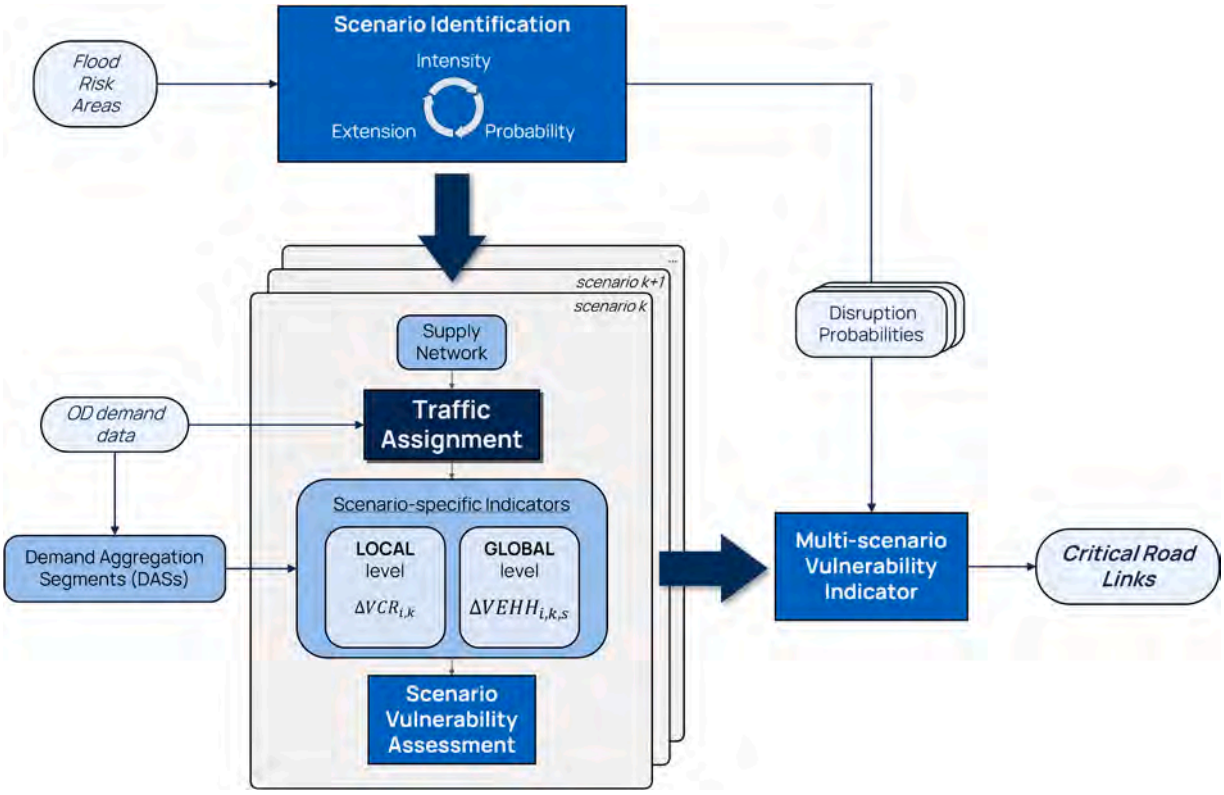

Fig. 1. Methodological Framework.

2020, Marian, Hijazi, Masad, and Abdel-Wahab, 2024)). Within this context, a common advancement is the explicit translation of predicted flood water depths to road speed reduction, via the use of functions or thresholds (Pregnolato, Ford, Wilkinson, and Dawson, 2017, Pregnolato et al., 2016), enabling analyses beyond pure link closures. Despite being more comprehensive than topological approaches, many applications of this kind produce aggregate, network-level vulnerability metrics, often emphasizing system-level performance losses, without fully assessing how specific vulnerabilities are distributed across links and travel segments.

Since flood hazards vary in extent, intensity and probability, multi-scenario analyses are increasingly used to avoid conclusions that depend on a single deterministic event. In the literature, scenarios are typically defined by return periods and flood extension (e.g., (Chen, Lu, Peng, and Ash, 2015, Shen and Kim, 2020, Borowska-Stefańska et al., 2025, Borowska-Stefańska et al., 2024)), by water-depth levels translated into link degradation/closures (e.g., (Pregnolato et al., 2016, Abdulla, Kiaghadi, Rifai, and Birgisson, 2020, Dong, Gao, Mostafavi, and Gao, 2022)), or by time-varying event representations that capture the event's evolution, as well as congestion dynamics (e.g., (Lin, Lu, Chen, and Brilakis, 2024)). These contributions show that impacts can be strongly non-linear across scenarios, especially in urban networks where rerouting and spillovers amplify local disruptions (e.g., (Marian, Hijazi, Masad, and Abdel-Wahab, 2024, Dong, Gao, Mostafavi, and Gao, 2022)). However, multi-scenario evidence is often handled in a fragmented way: results are frequently reported scenario-by-scenario, or aggregated ex post without an explicit treatment of hazard likelihood and uncertainty, which limits the ability to derive robust priorities for preparedness and mitigation under flood risk (e.g., (Shen and Kim, 2020, Borowska-Stefańska et al., 2025, Borowska-Stefańska et al., 2024)).

A common missing component of flood vulnerability studies in the literature is the limited exploration of demand heterogeneity. Most of the work keeps transport demand aggregated, implicitly assuming uniform exposure across trip types. Yet several contributions indicate that criticality rankings and impact patterns can change when analysis considers how trips differ by geography, trip length, or network dependency (e.g., (Dowds, Sentoff, Sullivan, and Aultman-Hall, 2017, Tsang and Scott, 2020)). In the context of flood events then, segmentation is particularly relevant because disruption impacts are distributive and thus, vulnerability assessment studies that account for demand heterogeneity can support more targeted policy measures.

Overall, few studies jointly adopt multi-scenario flood analyses that embed demand heterogeneity as a core analytical dimension of vulnerability assessment. When demand segmentation is considered, it is typically explored in controlled or test environments (e.g., (Dowds, Sentoff, Sullivan, and Aultman-Hall, 2017)), within accessibility-based analyses focused on specific destinations or services (e.g., (Shen and Kim, 2020, Loreti et al., 2022)), or with reference to particular population groups (e.g., (Crosson, Tong, and Zhang, 2020)). To the best of the authors' knowledge, no existing contribution assesses the systemic impacts of flood disruptions across multiple scenarios while explicitly analysing differentiated demand segments and identifying segment-specific critical road links within an urban road network.

Moreover, a relevant limitation is found in the context of application of flood vulnerability studies, as evidence of assessments for Italian metropolitan areas is still limited. For Milan specifically, to the best of the authors' knowledge, the most relevant contribution is a flood resilience-based cost–benefit analysis of the Malpensa Airport (Pagliara and Zingone, 2023), which does not model systemic flood vulnerability of the private road network, and it is limited in scope.

Table 1 highlights that, while multi-scenario flood analyses are increasingly adopted, demand heterogeneity is rarely accounted for as a core analytical dimension, and vulnerability metrics are predominantly at the system-level.

The reviewed literature suggests a clear methodological gap for dense metropolitan road systems exposed to flood hazard: integrating hazard maps with traffic modelling is increasingly common, and multi-

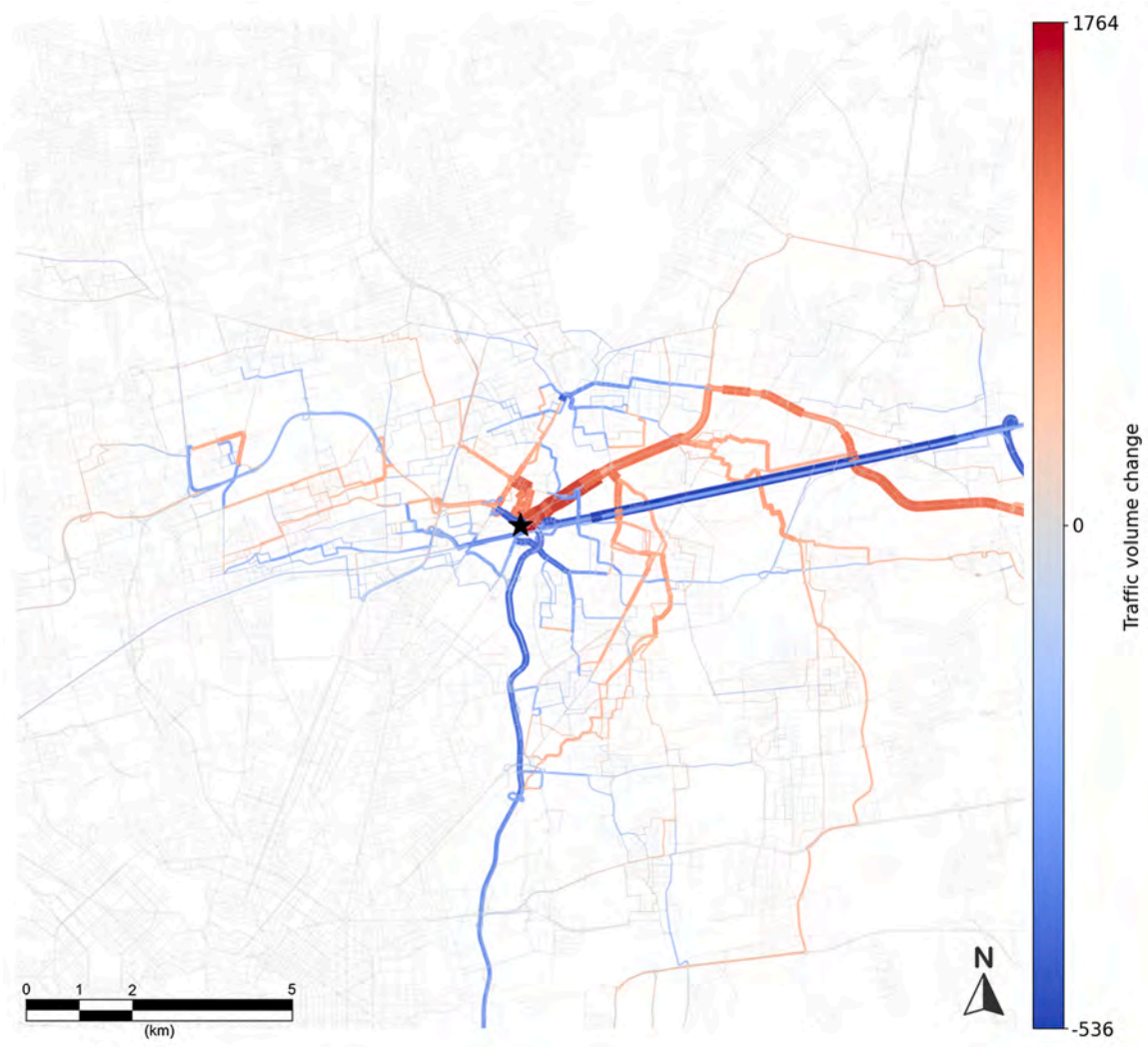

Fig. 2. Change in traffic volumes on paths using the starred road link between the base and a flood scenario. Blue denotes decreasing path volumes, and red denotes increasing path volumes.

scenario approaches are becoming more established, but:

- vulnerability indicators are mostly intended to reflect the overall network impacts of flooding, rather than identify specific critical points; this allows to assess and compare the systemic impact of hazardous events but hinders the policy maker's ability to extract information on the system weaknesses.
- demand heterogeneity remains understudied as a core analytical dimension, especially when the goal is to derive policy-relevant priorities and identify which network components are critical for different travel patterns.

Our study positions itself in this context by providing a multi-scenario, system-based assessment whose output vulnerability indicators are at the link-level and explicitly demand segment-specific. This work aims to provide a solid and replicable framework for the vulnerability assessment of urban road networks, enabling the design of targeted preparedness and mitigation strategies.

3. Methodology

The proposed methodological approach (Fig. 1) aims to combine geospatial flood data with a traffic assignment model, with the goal of identifying road links that become critical in the event of flooding due to the impact of traffic rerouting and congestion. This methodology relies on the identification and simulation of a set of flood scenarios, resulting from the combination of flood extension data with assumptions on discrete flood depth. Accordingly, the impact of flood-induced speed reduction on vehicles travelling on the network is assessed.

First, a set of flooding scenarios $K = \{k_1, k_2, \cdots, k_n\}$ is identified. As discussed in the previous section, flood risk areas provide information on the extension and the relative probability of an event's occurrence. Several water depths are also assumed; this information, combined with the flood risk areas, allows to identify flood scenarios. Therefore, each scenario k is identified by a water depth for each risk area: $k = \{(A_1 : depth_1), \cdots, (A_n : depth_n)\}$. Following the hypothesis that there is a relationship between the water depth and the maximum speed that can be reached by a vehicle (see Eq. (8)), the supply model is modified accordingly.

In addition to being the input for the traffic assignment model, demand data are used to extract a set of Demand Aggregation Segments (DAS) $S = \{s_1, s_2, s_3\}$, which constitute the core analytical units of the vulnerability assessment. Each DAS constitute a demand segment characterised by similar travel patterns and/or behavioural attributes, such as purpose of travel or age category, allowing network performance and vulnerability to be evaluated from the perspective of distinct demand profiles. This methodological choice allows to highlight segment-specific critical roads that would otherwise be concealed if demand were

to be treated as homogeneous. In aggregate analyses, vulnerability rankings are typically dominated by the most prevalent travel patterns, yielding a single set of "globally" critical roads. In contrast, the proposed approach supports a more differentiated interpretation of vulnerability, enabling decision-makers to prioritise preparedness and mitigation measures according to the demand segments most exposed to flood-induced disruption.

The traffic assignment model of each $k-th$ flood scenario will characterize each road link i with a $q_{i,k}$ level of vehicular traffic flow and a C_i level of capacity (expressed in terms of vehicles that can pass through it in the specified time frame of analysis). Thus, the volume-capacity ratio (VCR) of a road link i in scenario k can be defined as,

$$VCR_{i,k} = q_{i,k}/C_i \tag{1}$$

This indicator is a commonly used metric for modelling the level of congestion of a network edge or node (Lyman and Bertini, 2008) and it is frequently used in vulnerability assessment to identify network elements that become overly saturated in the case of a disruption. The VCR is a metric that analyses traffic flows on the **Local level**, providing insights strictly related to the element's functioning inside the operating conditions of the whole system. Indeed, such a metric address whether a road is problematic in terms of capacity or if the demand to use that road is too high (or too low), but it does not encompass the systemic relevance of that specific road inside the system. As such, other measures that inform about the relevance of a network link in the whole system on a **Global level** are also used in the literature. For example, Scott et al. (Scott, Novak, Aultman-Hall, and Guo, 2006) have proposed a network robustness index that models the importance of a given network link to the overall system as the change in travel-time cost associated with re-routing all traffic in the system should that road segment become unusable. This index represents the change in vehicle-hours travelled on the network following the closure of a specific link.

In the context of this work, said index was slightly conceptually adapted to reflect the desired informative output of the analysis. In other words, the **Global level** analysis of the presented methodological approach does not aim to assess the systemic impact of a targeted failure, as the network robustness index proposed by Scott et al. aims to do, but rather, its goal is to assess the systemic importance of a link regardless if that link is impacted or not. As such, the following metric is proposed,

$$VEHH_{i,k,s} = \sum_{j \in g_i} h_{j,k,s} \cdot t_{j,k} \tag{2}$$

where $h_{j,k,s}$ is the traffic flow on the $j-th$ path, in the $k-th$ scenario, and related to the $s-th$ DAS; $t_{j,k}$ represents the time required to complete the $j-th$ path under the $k-th$ scenario; and g_i represents the set of network paths that run through the $i-th$ link.

This indicator indeed combines the total flow of all paths that use that link with the travel time needed to complete those paths, thus providing a metric of systemic relevance. It allows for the twofold assessment of how relevant a link is in the path choice of road users inside the overall system, as well as the estimate of the travel times associated with those paths, as calculated by the traffic assignment model. On its own, the Eq. (2) is able to pinpoint critical network sections that are responsible for *"conducting"* high levels of demand, as well as longer trips that, in the case of disruption, will have to be rerouted and thus, may create great perturbation effects to the system.

Additionally, Eq. (2) is defined to be dependent on each DAS's demand level; in doing so, it is possible to highlight the criticality level of a road link also based on the relevance given to it by each DAS. Thus, while Eq. (1) is strictly related to *localized* levels of congestion, Eq. (2) represents the *systemic* change in user behaviour and travel patterns in the network.

Being the present application a multi-scenario assessment, Eqs. (1) and (2) were also defined in relative terms in order to model the impacts of the $k-th$ flood scenario with respect to the *base* scenario.

$$\Delta VCR_{i,k} = VCR_{i,k} - VCR_{i,base} \tag{3}$$

$$\Delta VEHH_{i,k,s} = VEHH_{i,k,s} - VEHH_{i,base,s} \tag{4}$$

Eqs. (3) and (4) can indeed assess the **Local** and **Global** effects, respectively, of a targeted or diffused disruption.

For improved clarity, a visual representation of the differential traffic flows that constitute the proposed indicator at Eq. (4) is provided at Fig. 2. The figure allows to understand how the paths that take a specific road link change, in terms of origin and destination and volume, in the event of flooding.

Subsequently, values from Eqs. (3) and (4) are normalized and combined into a single scenario-specific vulnerability metric $SV_{i,k,s}$:

$$SV_{i,k,s} = \sqrt{\Delta VCR_{i,k}{}^2 + \Delta VEHH_{i,k,s}{}^2} \tag{5}$$

where:

$$\Delta VEHH_{i,k,s} > 0$$

$$\Delta VCR_{i,k} > 0$$

In doing so, by applying Eq. (5) to a network-wide disruption k it is possible to pinpoint those network elements that become both more congested and more relevant in user path choices of each DASs. Thus, affecting global performances due to changes at a local level. Although informative in the case of a specific scenario, in the context of a multi-scenario application, Eq. (5) must also be extended to consider the different probabilities of occurrence of disruptive events, in order to provide a single vulnerability value in the case of a stochastic hazardous event. As such, the following vulnerability indicator is defined:

$$V_{i,s} = \sum_{k \epsilon K} SV_{i,s,k} \cdot w_k | SV_{i,k,s} \; \epsilon \; \overline{SV_{i,s}}, \; w_k \; \epsilon \; \overline{W} \tag{6}$$

with $\overline{SV_{i,s}}$ being the vector of scenario-specific vulnerabilities (Eq. (5)), and $\overline{W}$ being the vector of scenario probabilities or frequencies of occurrence.

By doing so, all the scenario-specific vulnerabilities of each road link are combined using a set of stochastic weights related to the actual occurrence of the hazardous event. By combining these values, the events with the highest probability will count more towards the identification of vulnerable links, allowing to dampen assessment results from less likely scenarios, whose higher expected disruptive effect, can overestimate vulnerabilities, skewing the results, and thus hindering an informative outcome. Additionally, this metric is DAS-specific, enabling the extraction of more targeted information on the actual vulnerabilities linked with typical travel behaviours and patterns.

In summary, Eq. (6) is a vulnerability metric that leverages traffic flow analysis at both the local and global levels to identify demand-specific systemic vulnerabilities at the link level. Its application focuses on assessing changes in congestion and link utilisation under spatially diffused disruptive events, explicitly accounting for differences in severity, spatial extent, and probability of occurrence. The indicator is intentionally based on well-established traffic performance measures, as the objective is not to model full resilience dynamics (i.e., both the initial shock and the system's functional recovery over time) but to support the identification and prioritisation of road links that become critical due to the combined effect of local congestion increase and systemic traffic rerouting under flooding.

4. Case study

Milan is one of Italy's main financial, industrial and commercial centres, making it a key player on the national and European stage. The city is characterised by high urban density and a mature infrastructure network. The urban area serves as an important national transport hub,

Table 2
Link type features of the supply model.

Link Type	Name	Lane capacity [veh/h]	Max Speed [km/h]	# Links	Extension [km]
1	Motorway	1500	130	7041	1073
2	Trunk	1500	110	6117	583
3	Primary	1300	70	26,246	929
4	Secondary	1000	50	40,762	1286
5	Tertiary	800	45	264,964	9847

hosting major road, rail and air links throughout the region, with significant economic consequences. This context highlights the need to maintain solid operational capacity in the face of external stress factors, such as extreme weather events.

Despite its inland location, Milan is an interesting case study in urban flood challenges, thanks to a combination of historical hydraulic and modern urban development. The city is crossed by several waterways, the most important of which are the Seveso and Lambro rivers. Historically, heavy rainfall has led to recurrent river flooding, as these rivers exceed their capacity, particularly in the northern and eastern parts of the city. Complicating the situation, the dense and highly impermeable surface exacerbates sudden urban floods, where intense rainfall quickly overloads the existing urban drainage system. These events disproportionately affect crucial transport corridors, including crucial tunnels, arterial roads, and access points to motorways, causing widespread traffic disruption.

4.1. Overview of the transport simulation framework

The analysis is based on a transport simulation model, developed using PTV VISUM© software, that simulates private transport traffic flows during the morning peak hour, from 8:00 a.m. to 9:00 a.m. The study area includes the city of Milan itself, some municipalities in the Milanese hinterland, the city of Monza and other municipalities in the province of Monza and Brianza. It contains 610 internal zones, and 29 external ones, all provided by AMAT (*Agenzia Mobilità Ambiente Territorio*). The hourly origin-destination (OD) trip matrix has been taken from the Lombardy Region open dataset.

The road network model was extracted from *OpenStreetMap* data, down to the level of the detailed urban road network, with a total of 232,706 nodes and 579,956 links, classified into 6 road types, illustrated in Table 2, along with their main characteristics of lane capacity and speed limit. Capacity values (veh/h per lane) follow standard practice in transport engineering. Base per-lane capacity ranges are taken from the Highway Capacity Manual (Comune di Milano 2022) that reports typical capacities of about 1800–2400 veh/h per lane on free-flow motorways, decreasing for urban trunk roads and local streets depending on the geometry. For this study, capacities representative of an urban metropolitan context (Table 2) are taken, which are conservative with respect to HCM lane capacities in order to reflect the effects of urban access, frequent junctions and freight traffic.

Volume delay functions are defined for each link type: motorways, trunk, primary, secondary and tertiary. The assignment model is carried out using a Stochastic User Equilibrium (SUE) for congested systems (Cascetta, 2009).

4.2. Demand aggregation segments

Consistently with the methodological framework introduced in the previous Section, the case study adopts a Demand Aggregation Segment

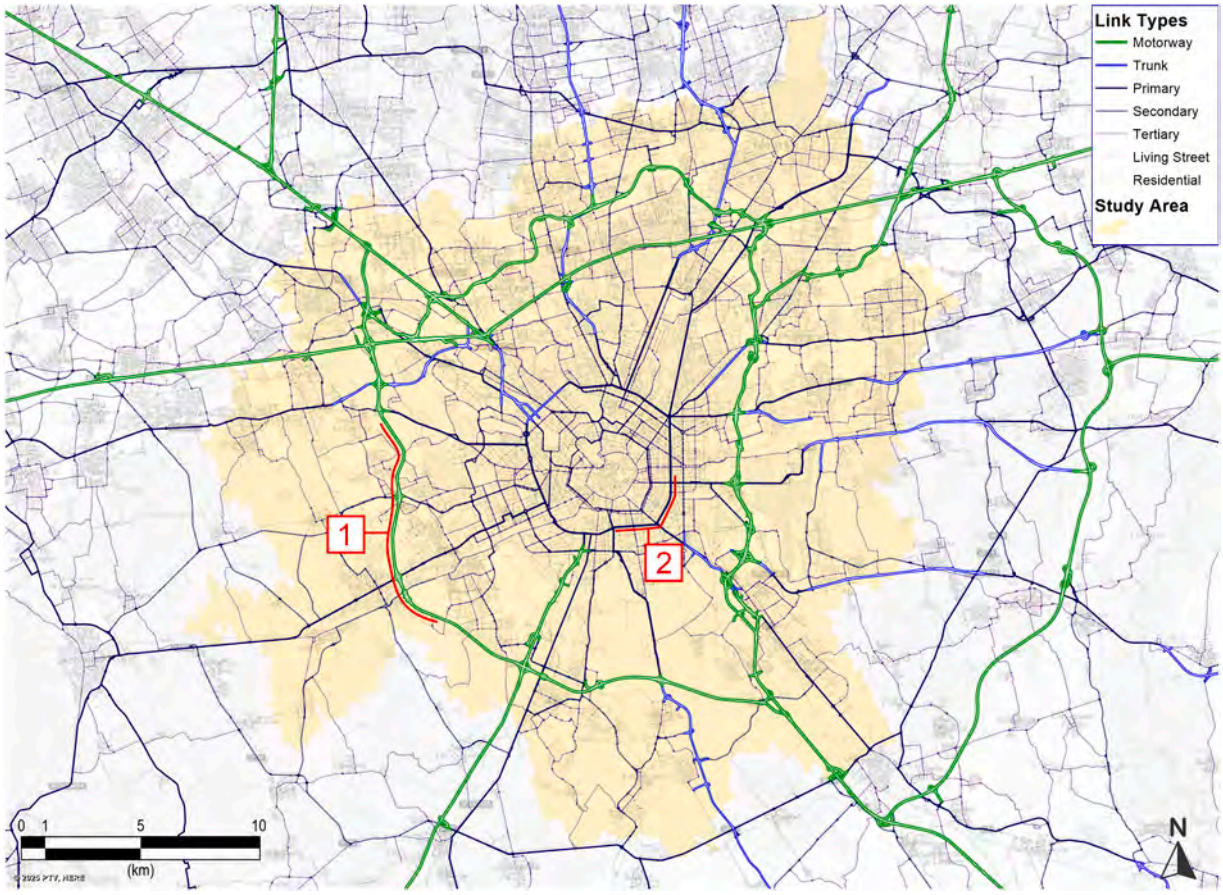

Fig. 3. Study area and road network. Number 1 marks a section of the *Tangenziale* (outer ring road). Number 2 marks a section of the *Circonvallazione* (inner ring road).

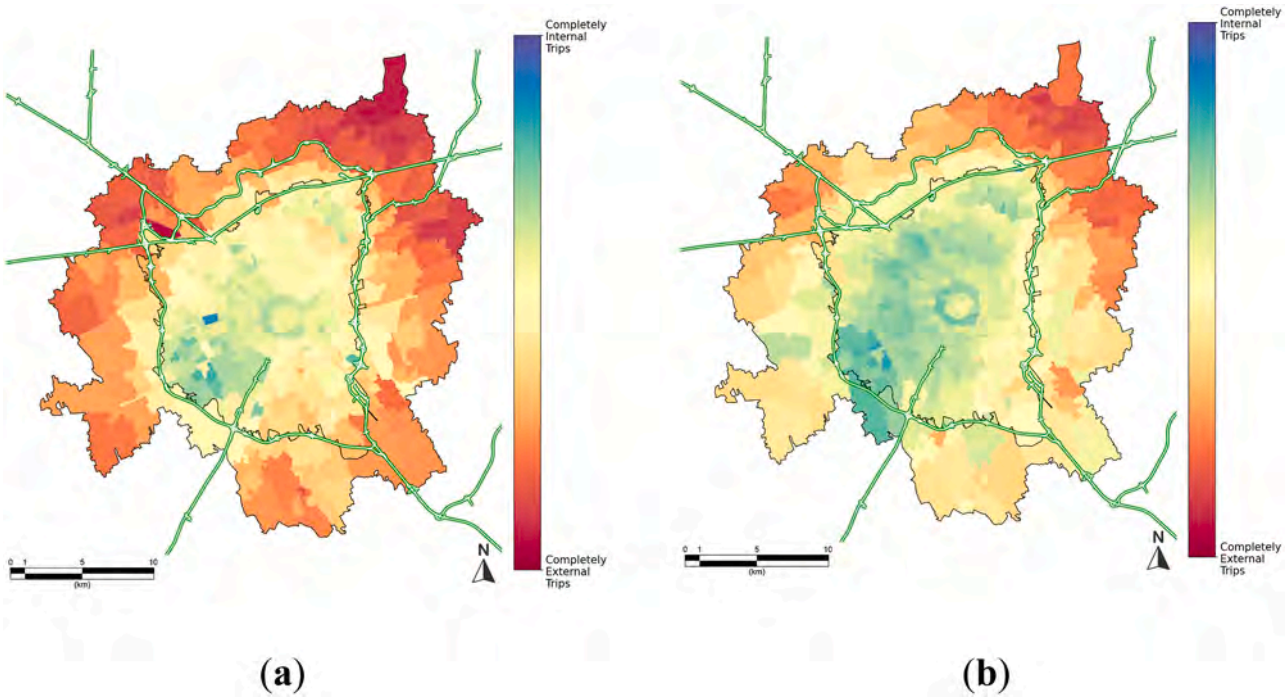

Fig. 4. Share of (a) generated and (b) attracted demand by area.

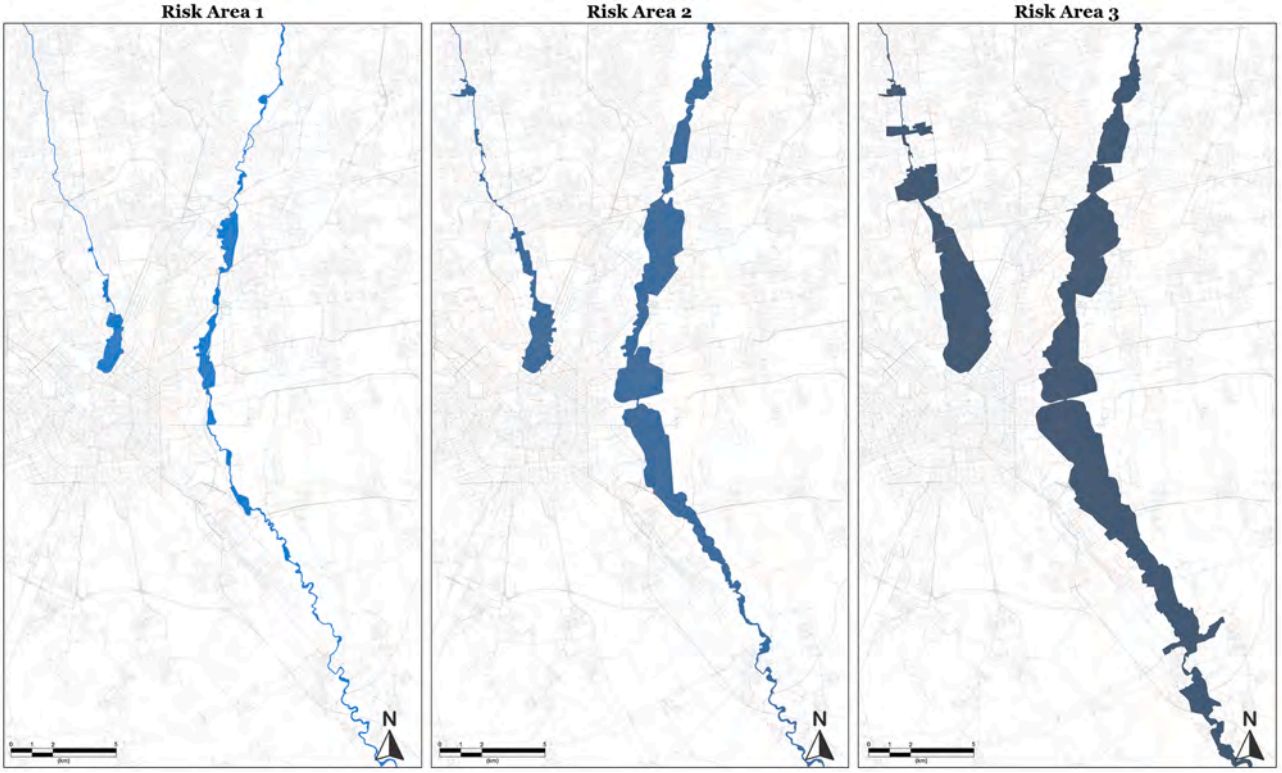

. 5. River courses and Risk Areas.

(DAS) structure designed to capture differences across user groups.

For this case study, demand is segmented using a purely geographical criterion, based on the relative location of origin and destination zones with respect to a strategic urban boundary. This allows demand to be grouped into a set of DASs that reflect typical travel patterns. This choice is motivated by two main considerations. First, a geographically based segmentation is straightforward, easily interpretable, and readily transferable, making it well suited to support the application of the proposed methodology, which explicitly relies on demand heterogeneity. Second, this segmentation is representative of the dominant travel patterns observed in metropolitan areas characterized by a radial–ring road structure, such as Milan, where morning peak-hour traffic features

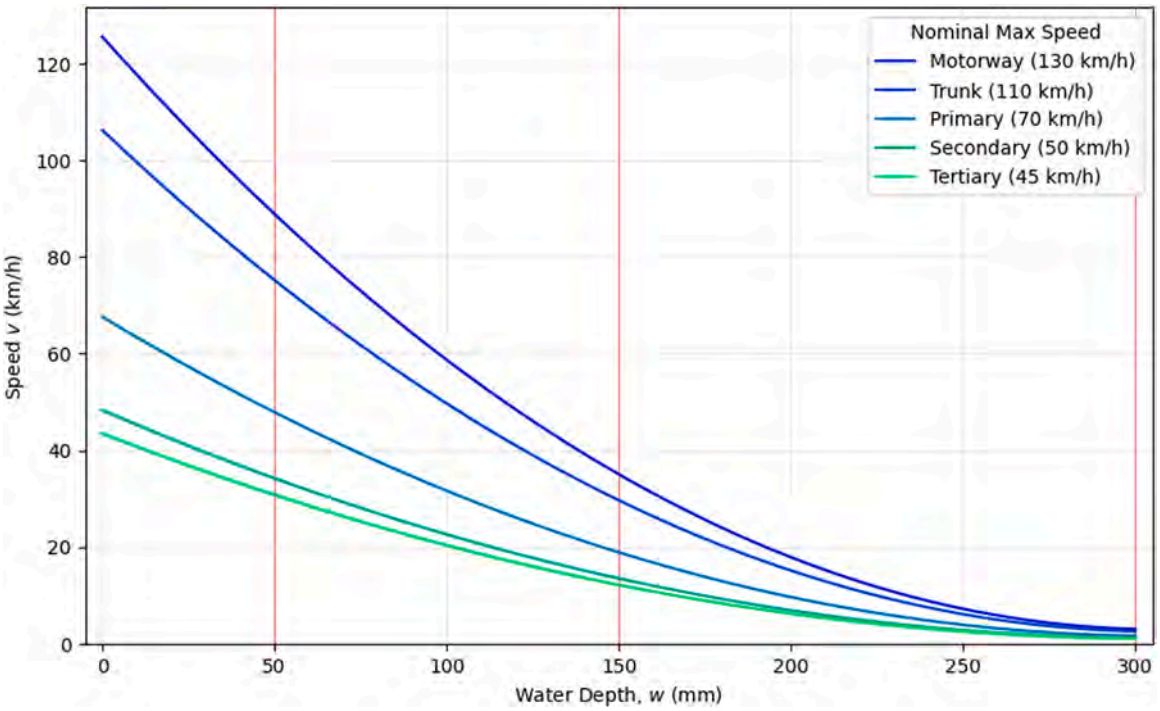

Fig. 6. Maximum vehicle speed reduction as a function of water depth (Eq. (8)) relative to the model's link types. Discrete water depths used in flood scenario modelling are represented by the red vertical lines.

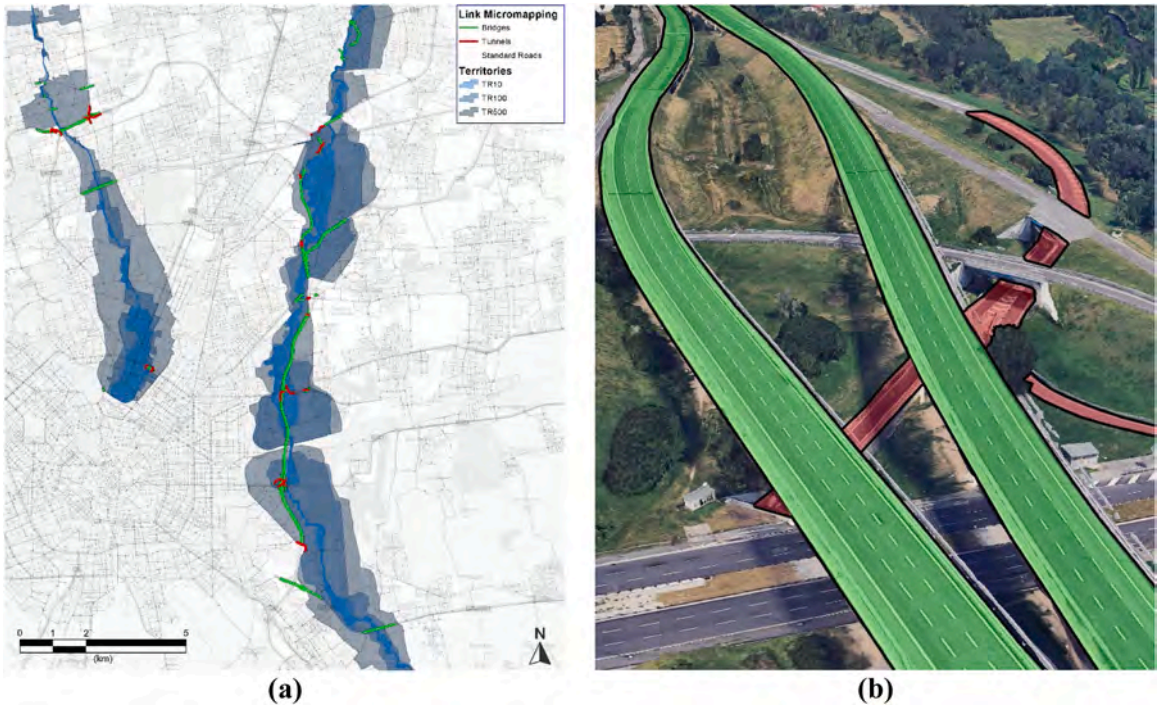

Fig. 7. Micro-mapping of bridges and underpasses. (a) Location in the study area, (b) detailed example of the ring road - Viale Enrico Forlanini junction.

inbound commuter flows, urban congestion, and passing traffic along major regional and national roads.

In practical terms, the segmentation is implemented using Milan's *Tangenziale* road (Fig. 3) as the dividing boundary, identifying internal and external zones. The *Tangenziale* represents the high capacity outer ring road that separates the dense urban core from the surrounding metropolitan and suburban territory. More importantly, this boundary distinguishes trips that are structurally dependent on crossing or using the ring road from those that are not, thereby identifying users who are more constrained in their routing options when flood-induced disruptions affect radial access roads and ring-road interchanges.

Based on this criterion, the overall OD matrix is segmented into three mutually exclusive DAS. **Intra-ring (II)** trips occur between internal zones and represent predominantly local movements within the urban core. These trips tend to rely on lower-capacity roads, such as the historical ring road (*Cerchia dei Bastioni*), the more modern inner ring road

Table 3
Scenarios identification with water depth for each area.

Scenario	Area 1	Area 2	Area 3
Sc1	50 mm	0 mm	0 mm
Sc2	150 mm	50 mm	0 mm
Sc3	300 mm	150 mm	50 mm
Sc4	300 mm	300 mm	150 mm
Sc5	300 mm	300 mm	300 mm

(*Circonvallazione*), and their associated radial connections. **Inter-ring (EI)** trips are defined between internal and external zones and largely represent commuter flows that must cross the *Tangenziale* or use a portion of it. **External–External (EE)** trips occur between external zones and include passing, or peripheral and long-distance traffic flows that are most likely to take the *Tangenziale* (Fig. 4).

While implemented here for the Milan case study, this segmentation approach is transferable to a wide range of large metropolitan areas characterised by a predominantly flat morphology and a ring-road system that functions both as a connector and as a bypass of the urban core.

4.3. Flood area extension and probability

The hydrological vulnerability of Milan's transport system is intrinsically linked to its two main waterways: the Seveso River and the Lambro River. Both rivers originate in the Lombardy Pre-Alps and cross the metropolitan area along largely artificial and heavily constrained routes. The Seveso is known for its high hydraulic instability; in the urban section, its course is mainly underground and channelled for several kilometres, intersecting the city from north to south in a radial pattern. This hydraulic bottleneck configuration is the main cause of historical flooding, directly affecting the road network, as its floods tend to quickly inundate low-lying areas, such as underpasses and crucial road intersections. On the other hand, the Lambro largely marks the eastern boundary of the city, running along the eastern section of the ring road, and although its hydraulic impact is greater in the peripheral areas, its flooding frequently threatens important connections between the urban, suburban and rural areas.

The flood hazard maps used in this study were developed by the Po River Basin Authority (ADBPO), a public body responsible for coordinating and implementing river basin management and flood risk management at the district scale, including the development of basin plans, hazard and risk mapping, and the oversight of measures aimed at protecting water resources and reducing hydrogeological risk.

These cartographic data were developed in 2020 in accordance with the EU Floods Directive (2007/60/EC) (Autorità di Bacino Disrettuale del Fiume Po (ADBPO) 2020), and are characterized by a flood event probability, expressed through the *Time of Return* (TR), which is a statistical measure (in years) indicating the expected average time interval between the occurrence of two events of equal or greater intensity. Flood extents are derived from hydrological–hydraulic modelling for primary river networks and from geomorphological or historical data where detailed modelling is not available, providing a district-level representation of the risk of flooding.

The official maps provide three risk areas, shown in Fig. 5, each associated to a different TR.

- **Area 1:** identifies a high probability scenario ($TR = 10$ *years*), a frequent event with an annual probability of occurrence of 5%.
- **Area 2:** identifies a medium probability scenario ($TR = 100$ *years*), it is a standard reference for planning, with an annual probability of occurrence of 1%.
- **Area 3:** identifies a low probability scenario ($TR = 500$ *years*), that describes extreme event with an annual probability of occurrence of 0.5%.

Table 4
Simulation scenarios and associated return periods.

Scenario	Return [years]
Sc1	10
Sc2	100
Sc3	500
Sc4	1100
Sc5	1650

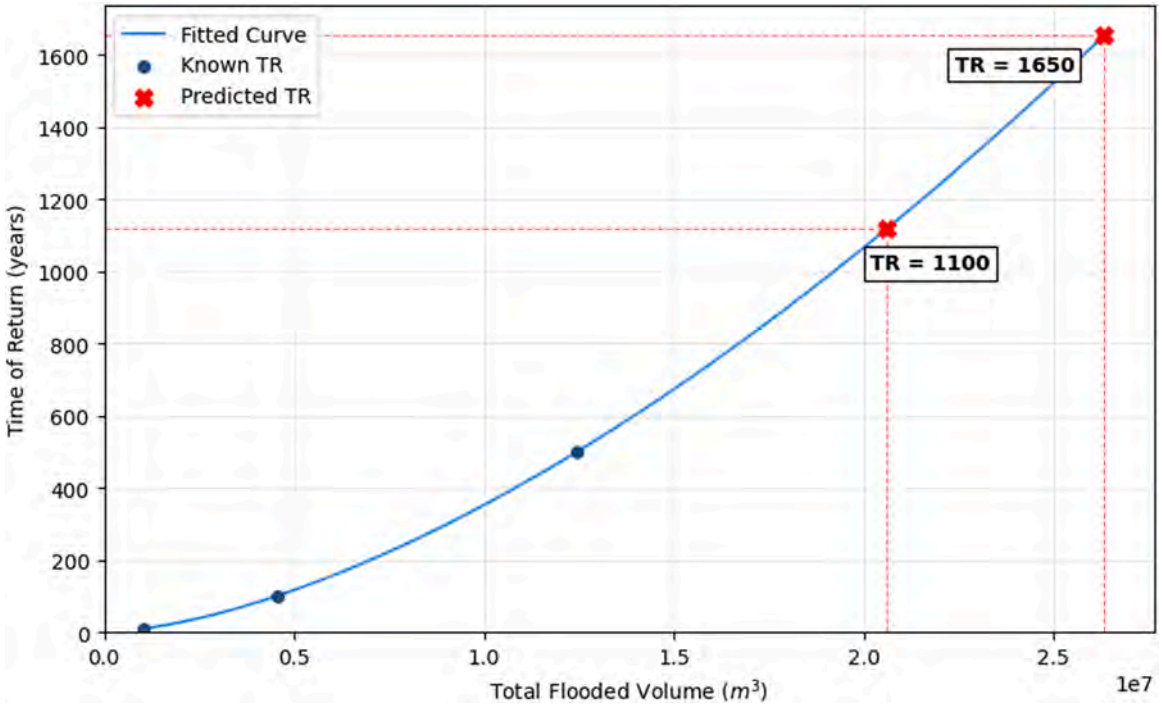

Fig. 8. Time of Return inference for Sc4 and Sc5, as a function of the computed flood volume.

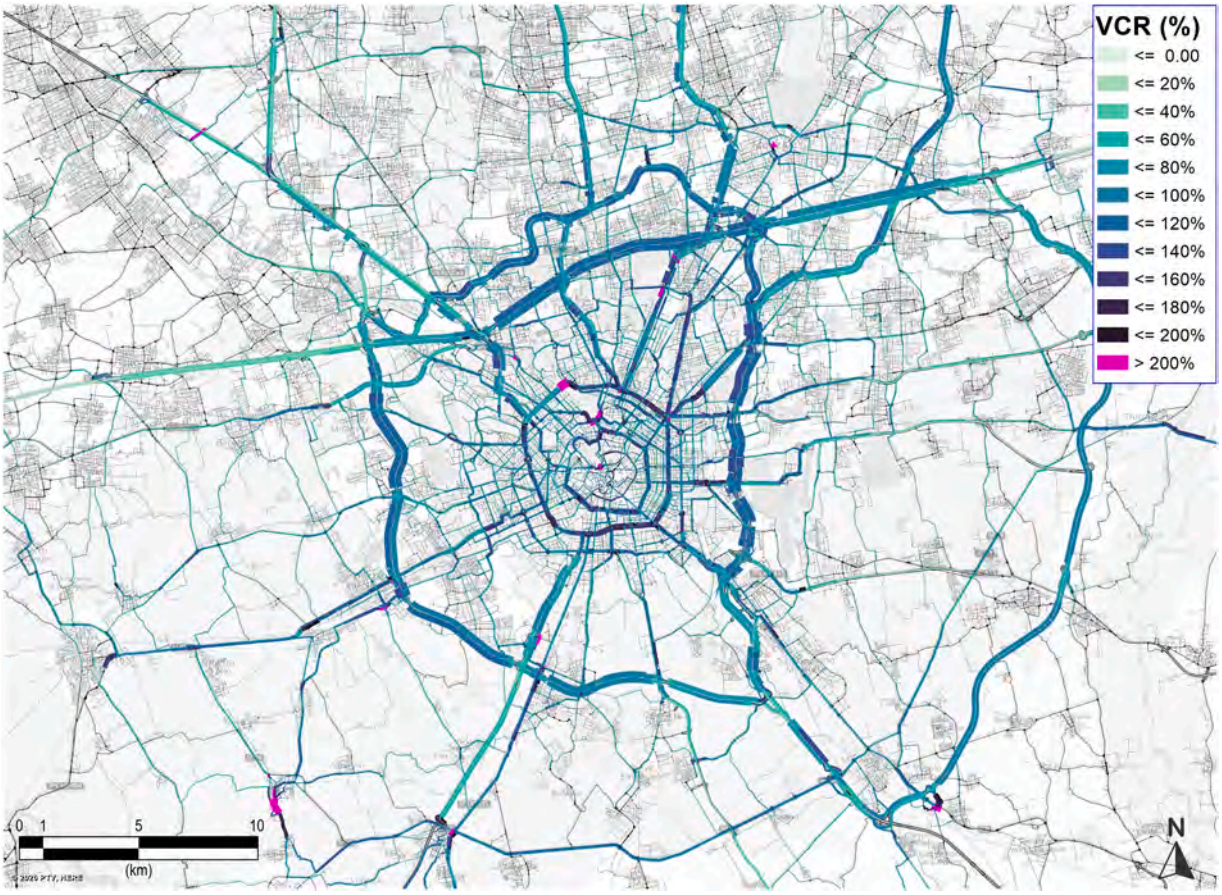

Fig. 9. Traffic Assignment result of the Base Scenario. The thickness of each bar is directly proportional to the traffic volume on the link.

Table 5
Comparison of total vehicles-hours and vehicle-kilometers travelled across scenarios.

	VEHH	Δ*VEHH* (%)	*VEHKM*	Δ*VEHKM* (%)
Base	102,046	-	4558,939	-
Sc1	104,401	2355 (2.3%)	4588,337	29,398 (0.6%)
Sc2	107,285	5239 (5.1%)	4613,093	54,154 (1.2%)
Sc3	123,584	21,538 (21.1%)	4746,002	187,062 (4.1%)
Sc4	154,520	52,474 (51.4%)	4967,961	409,022 (9.0%)
Sc5	179,460	77,414 (75.9%)	5127,908	568,968 (12.5%)

Table 6
Comparison of demand-weighted travel times [min] across scenarios and DASs.

	$\overline{T_{EE}}$	$\overline{\Delta T_{EE}}$ (%)	$\overline{T_{II}}$	$\overline{\Delta T_{II}}$ (%)	$\overline{T_{EI}}$	$\overline{\Delta T_{EI}}$ (%)
Base	31.2	-	10.6	-	27.4	-
Sc1	31.7	0.6 (1.9%)	10.8	0.2 (2.3%)	28.1	0.7 (2.7%)
Sc2	32.4	1.3 (4.0%)	11.2	0.6 (6.0%)	29.0	1.6 (5.8%)
Sc3	36.6	5.4 (17.3%)	13.0	2.5 (23.3%)	33.9	6.5 (23.6%)
Sc4	45.3	14.1 (45.3%)	15.9	5.3 (50.4%)	42.7	15.3 (55.6%)
Sc5	51.5	20.3 (65.1%)	19.5	8.9 (84.2%)	49.7	22.3 (81.4%)

4.4. Flood intensity: linking water depth and speed reduction

As briefly explained in the methodology, it is required to identify distinct scenarios that simulate network performance degradation across varying flood spatial and intensity dimensions. Given the focus on network vulnerability, scenarios are constructed by coupling a predefined flood risk area, with a specific uniform water depth on the affected road segments within that area. It is acknowledged that actual flood events result in highly variable water depths across an inundated area. However, in the absence of raster flood data, a simplified and conservative approach is adopted. We assume a single fixed depth value of water for all affected road links within a defined floodable area, allowing for a controlled, reproducible, and comparative analysis between different severity levels.

Table 7
Comparison of demand-weighted travel distances [km] across scenarios and DASs.

	$\overline{L_{EE}}$	$\overline{\Delta L_{EE}}$ (%)	$\overline{L_{II}}$	$\overline{\Delta L_{II}}$ (%)	$\overline{L_{EI}}$	$\overline{\Delta L_{EI}}$ (%)
Base	25.6	-	5.8	-	19.6	-
Sc1	25.8	0.2 (0.8%)	5.8	0.0 (0.0%)	19.7	0.1 (0.5%)
Sc2	26.0	0.4 (1.6%)	5.9	0.1 (1.7%)	19.8	0.2 (1.0%)
Sc3	26.7	1.1 (4.3%)	6.0	0.2 (3.4%)	20.4	0.8 (4.1%)
Sc4	27.9	2.3 (9.0%)	6.2	0.4 (6.9%)	21.3	1.7 (8.7%)
Sc5	28.6	3.0 (11.7%)	6.4	0.6 (10.3%)	22.2	2.6 (13.3%)

To translate water depth into a quantifiable measure of performance loss, this study builds upon the framework proposed by Pregnolato et al. (Pregnolato, Ford, Wilkinson, and Dawson, 2017), which establishes a relationship between flood depth (w) and the maximum vehicle speed (v) that ensures safe driving (Eq. (7)). In the present work, this relationship has been used to express the impact of water depth on maximum vehicle speed reduction relative to the nominal, *unflooded* ($w = 0$) speed (Eq. (9)). Henceforth, this relationship can be applied consistently across flood scenarios to model the maximum speed at the link level (Fig. 6). The supply model is modified accordingly.

$$v_{ref}(w) = 0.0009w^2 - 0.5529w + 86.9448 \quad (7)$$

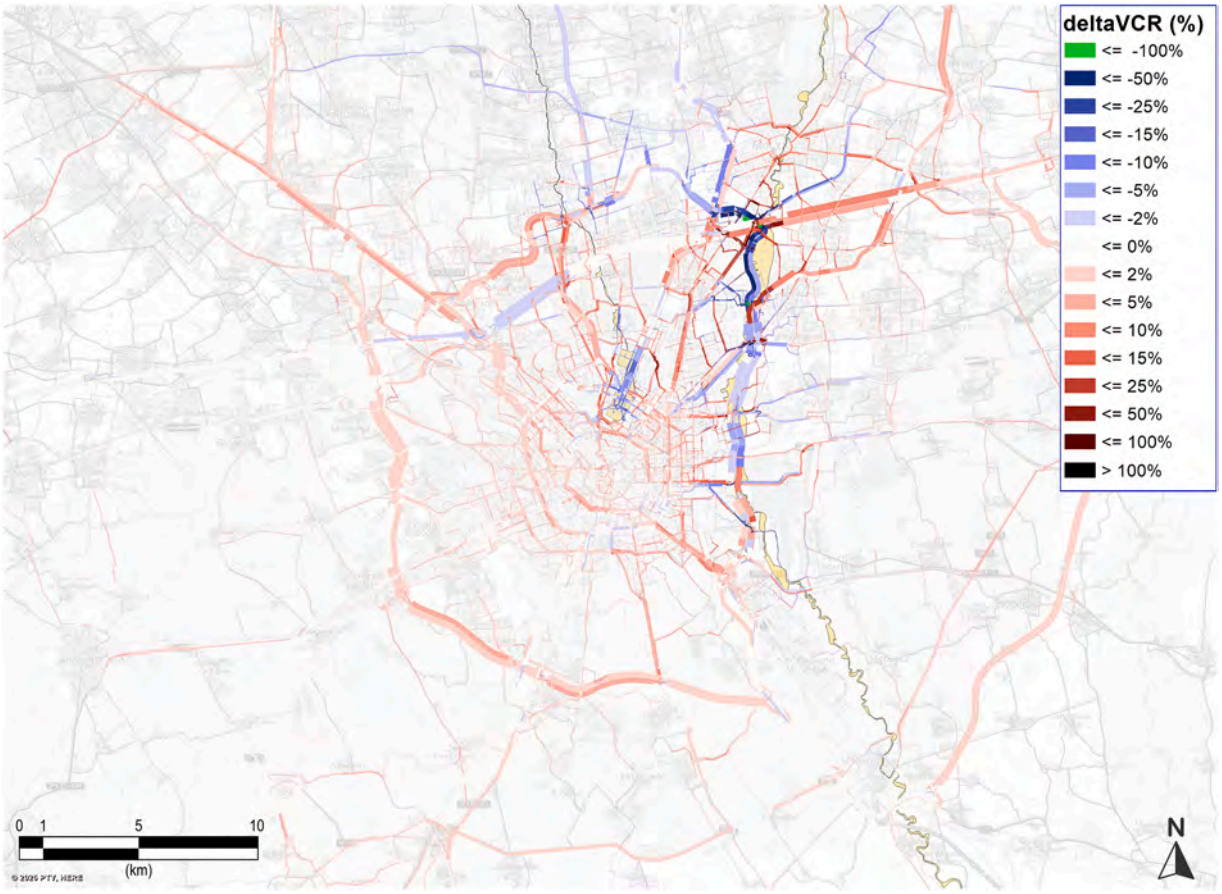

Fig. 10. Difference flow diagram for Flooding Scenario 1.

$$v(w, v_0) = v_0 \cdot \frac{v_{ref}(0)}{v_{ref}(w)} \tag{8}$$

Three representative water depths of 50 mm, 150 mm, and 300 mm, were selected to characterize distinct thresholds of flood impacts on road vehicle speed. These values reflect common thresholds observed in both experimental and numerical research. At approximately **50 mm**, surface water begins to significantly affect the tyre-road interaction, reducing friction and increasing the risk of aquaplaning at moderate speeds. Research by Rose & Gallaway (Rose and Gallaway, 1977) and Cerezo & Gothie (Cerezo and Gothié, 2009) has shown that even shallow layers of water cause a rapid reduction in skid resistance and increased susceptibility to aquaplaning, forcing drivers to significantly reduce their speed. At around **150 mm**, the hydrodynamic effects become more critical. The same Pregnolato et al. (Pregnolato, Ford, Wilkinson, and Dawson, 2017) has shown that buoyancy forces begin to counteract the weight of the vehicle, while drag forces increase significantly, making it difficult to maintain control. These conditions are associated with a significant reduction in vehicle speed, steering stability and braking effectiveness. Finally, **300 mm** represents a critical threshold at which the majority of passenger vehicles become unstable or begin to almost float. Computational and laboratory studies by Al-Qadami et al. (Al-Qadami et al., 2022) suggest that drag and lift forces at this depth can overcome vehicle weight and tyre adhesion, making continued motion unsafe.

4.4.1. Micro-mapping

The flood risk areas considered in this study refer to the flood probability at the ground level. In reality, not all road sections within a flood-prone area are equally affected: some are elevated above ground level, while others are below. To accurately represent these conditions, a detailed mapping process was carried out, as shown in Fig. 7. Roads built above ground level, such as bridges and overpasses, and those below ground level, such as underpasses, are identified. Bridges were assumed to remain unaffected under all flooding scenarios, as their elevation prevents any direct impact from floodwaters. Conversely, underpasses were considered to be fully disrupted and consequently closed to traffic even under minor flood events.

This differentiation allows to account for specific network features, such as the fact that a large portion of Milan's *Tangenziale* is elevated above ground level. As a result, this section of the network remains operational during flood events, even though it lies almost entirely within identified flood risk areas, thus maintaining continuity of north–south traffic flows. On the contrary, several entry and exit ramps along that same *Tangenziale* will be permanently closed under flooding scenarios, as parts of them are located in underpasses.

4.5. Definition of simulation scenarios

The previous sections introduced the three areas, defining their spatial exposure to risk, probabilities, and three representative water depth levels. By combining these parameters, it is possible to construct an ordered set of five scenarios, as shown in Table 3, from minimal inundation (i.e., Scenario 1 "Sc1") to saturation of the entire area (i.e., Scenario 5 "Sc5"). For Sc1, Sc2, and Sc3, the Time of Return is directly inherited from the largest spatial extent affected, while for the last two scenarios, Sc4 and Sc5, the extreme flood events, a statistical inference is performed, based on the hypothetical relationship between flood magnitude and probability. The total flood water volume (V), intended as a proxy of the event's overall magnitude, is computed for Sc1, Sc2, and Sc3 based on the respective flood area extension and assigned discrete depths of each scenario. As such, a relationship of the form

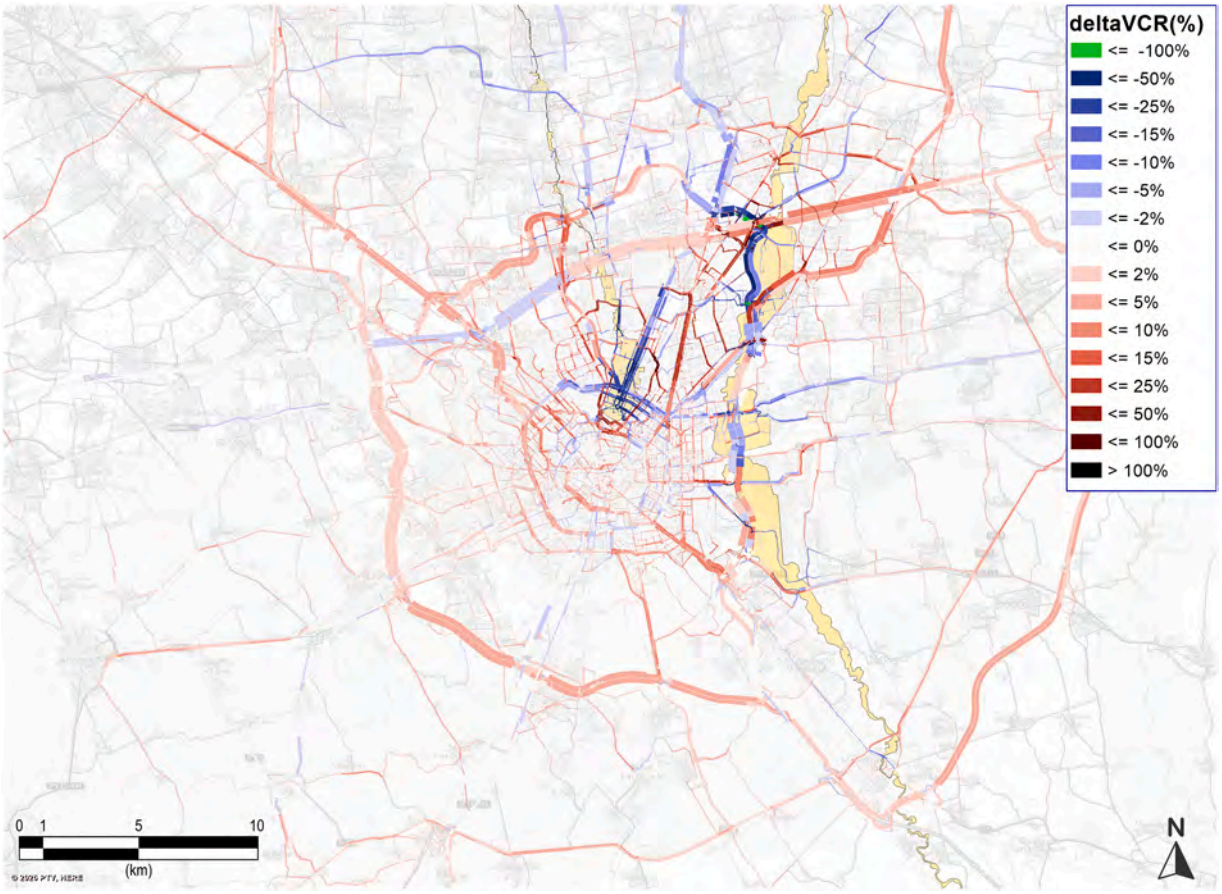

Fig. 11. Difference flow diagram for Flooding Scenario 2.

$TR = a \cdot V^b$, was fitted to the three known data points. In the end, the empirically derived function was then applied to the calculated volumes of the two extreme scenarios (being their flood area extensions known and water depth assumed), to quantitatively infer their Time of Return (Fig. 8 and Table 4).

$$TR(V) = 2.29 \cdot 10^{-9} \cdot V^{1.598} \quad (9)$$

5. Simulation results

Prior to discussing the expected impacts of these events on traffic, it is worth addressing the current picture of Milan's urban mobility. As shown in Fig. 9, the majority of car traffic is expected to be distributed along the outer ring road, since it is heavily used by the EE segment, and it also acts as a connector between multiple national highways, like the A1 Milan - Naples, the A7 Milan - Genoa and the A4 Turin - Venice. Though traffic flows are higher in the outer ring road, the inner one presents a higher degree of congestion, due to its lower capacity and the higher demand concentration.

Table 5 contains descriptive indicators obtained by the simulation of all the flood scenarios. It contains the overall *VEHH*[1] and *VEHKM*[2] of the system, as well as the average demand-weighed travel time of each DAS for every scenario. Absolute and relative variations with respect to the base scenario are also reported.

It can be noted that, given the variation of *VEHH* and *VEHKM*, minor flood events are not so disruptive to the urban mobility system on an aggregate scale, while adverse effects start to become much more significant starting from Sc3, when largest areas start to flood. Comparing the change in *VEHH vis-a-vis* the change in *VEHKM* it can also be observed that flooding induces a higher increase in travel time than to the increase in travelled distances. This result may indicate that Milan not only lacks capacity but also redundancy to overcome these types of events, as traffic flows are mainly forced to follow the same paths or are slightly re-routed, but take much more time to complete their journeys due to a higher level of congestion.

One can also observe that DASs are impacted differently across scenarios. In relative terms, average travel time of II and EI segments is more affected than EE's, perhaps due to a lack of road capacity in the urban core of the network, although the average travel time of EE segment is greatly impacted in absolute terms too (Table 6). Overall, EI segment comes out to be the most impacted segment in terms of travel time change, showing how mobility in and out of the city is particularly vulnerable to the flooding of major road links along the outer ring road.

In terms of average travelled distances, EE and EI are greatly impacted by flooding (Table 7). The inundation of main roads in the outskirts of the city forces flows to reroute to alternatives longer paths. The lower increase in average travel distances for internal flows (i.e., *II*) can be attributed to either a denser network in the city's urban core, and thus a higher availability of alternative paths slightly longer than those taken in the base case, or the inevitable presence of high congestion levels which force flows to take already saturated paths.

Attention should also be drawn to the change in travel patterns that occur in the study areas, as seen in Figs. 10–14, the presented sequence of difference flow diagrams shows how the traffic volumes and congestion level change in the flooding scenarios, compared to the base case.

As per the results presented in Table 5, traffic flows, as expectable, are not excessively disrupted when flooding occurs at shallower depths

[1] Vehicle-hours travelled
[2] Vehicle-kilometers travelled

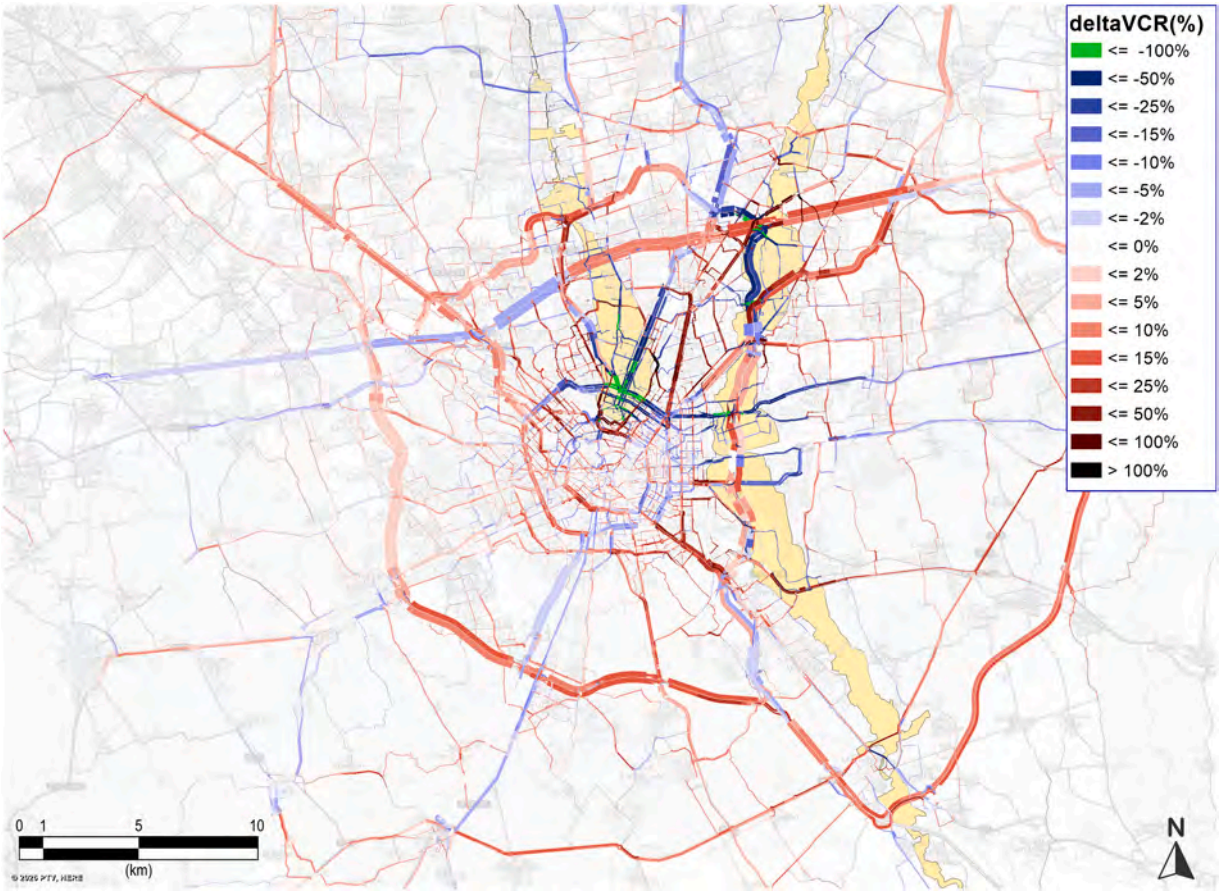

Fig. 12. Difference flow diagram for Flooding Scenario 3.

(i.e., Sc1 and Sc2). As Fig. 10 shows, the flooding of the Seveso River induces an increase of congestion in the surroundings areas, which start to become increasingly more impactful from the events severity described in Sc2. On the other hand, the flooding of the Lambro River in the eastern parts of the study areas force traffic slowdown along the ring road, forcing vehicles to re-direct to its northern section (which is also part of the national A4 highway) and to the secondary branch of the eastern ring road. Congestion, in some cases, will increase spill over to other, more distant and apparently less affected, parts of the network. For instance, the southern ring road sees a substantial increase of its *VCR*, as demand from the EE segment is redirected there, which heavily relies on ring roads for cross-city trips.

When flooding severity increases (i.e. starting from Sc3, where flood water depths are modelled to reach 300 mm in Area 1), car travel is expected to become completely hampered in the road links falling inside Area 1. This effect can be observed in Fig. 12, where certain road links are now void of volume. Notably, the northern ring road features a dual situation when comparing Sc3 with Sc4 and Sc5. In the former, this road still plays a funnelling role for traffic flows disrupted in other areas of the network, despite starting to flood in a small section; in the latter set of scenarios, instead, flood depths increase, making the highway much less performative in Sc4, and almost-completely unusable in Sc5. As a result, a substantial amount of flows are forced to exit the highway and either take the A54 or bypass the city using the southern ring road.

This assessment provides a sound basis for interpreting the results on a qualitative and level, by showing which links become more critical in the event of flooding. The difference flow diagram can be used to extract an overview of network criticalities, although it only gives an aggregate image of the system's equilibrium of a single probabilistic scenario. To investigate how specific demand segments are impacted and where systemic vulnerabilities arise in a multi-scenario framework due to uncertainty, it is necessary to carry out a quantitative vulnerability assessment. As such, in the next section, the methodology proposed in Section 3 will be applied and its results discussed.

6. Vulnerability assessment results

The methodological approach proposed in Section 3 is applied in order to identify the multi-scenario, demand-segmented systemic vulnerabilities of Milan's private transport system to the risk of flooding. The application of Eq. (6) allows for the assessment of both the local and systemic impact the flooding has on traffic flows by demand segment in a weighted multi-scenario framework. This indicator aims to identify the road links that are expected to become most critical under a spatially distributed hazardous event, such as flooding, due to the resulting degradation of road network performance. Identifying these vulnerable road links can therefore provide policymakers with actionable information to support preparedness measures aimed at mitigating the short-term impacts of flood-induced congestion.

Figs. 15 and 17 display the top three most vulnerable road segments for each DAS, each identified by a different colour, while in Table 8, the vulnerability index values, computed by applying Eq. (6), are reported.

First, it can be observed that most of the vulnerable links are concentrated along the outer ring roads and the radial access corridors in the north-eastern parts of the city or in the close proximity to it. As expectable, they are concentrated in and around flood areas, as these portions of the network are in the nearest to the impacted areas and thus are the first ones that have to accommodate for higher traffic volumes in the case of flooding.

Fig. 16 illustrates how the composition of the most vulnerable road links varies across demand segments in terms of functional road link type. As expected from a systemic analysis, vulnerability is shown to be

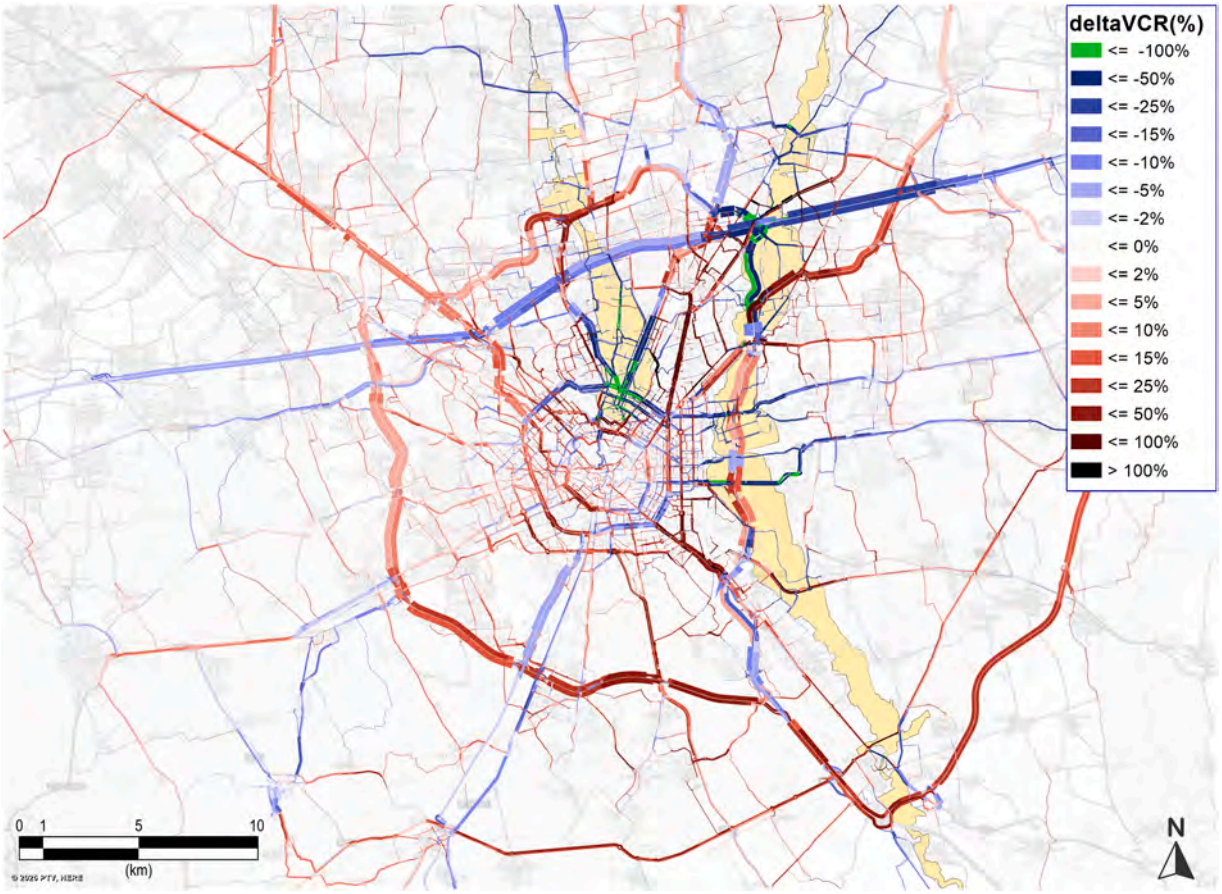

Fig. 13. Difference flow diagram for Flooding Scenario 4.

strongly shaped by the mobility patterns associated with each demand segment. For the External (EE) segment, vulnerability predominantly emerges on high-capacity infrastructure, indicating that flood-induced disruptions primarily affect strategic corridors supporting national and regional traffic. In contrast, vulnerability in the Intra-ring (II) segment is largely associated with secondary and tertiary roads, highlighting the critical role of the local road network in sustaining internal mobility under flooding conditions. This suggests that, for internal trips, link criticality does not necessarily coincide with high-capacity infrastructure but instead arises from localized congestion effects within the urban street network. The Inter-ring (EI) segment exhibits an intermediate configuration, reflecting its hybrid travel patterns and reliance on both higher-capacity and local road infrastructure. These results highlight the importance of demand segmentation in vulnerability assessment, as it directly influences which components of the road network are identified as critical and, consequently, which types of preparedness and mitigation measures may be most effective, depending on the road type.

Table 8 highlights marked differences in vulnerability levels across demand segments, with road links associated with the EE and EI segments exhibiting substantially higher criticality than those identified for the II segment. These differences reflect distinct vulnerability patterns associated with demand composition and functional and topological network characteristics. For the EE and EI segments, higher vulnerability levels are primarily driven by large absolute increases in travel times under flooding conditions, which strongly affect the $\Delta VEHH$ component of the vulnerability indicator (see Eq. (5)). This effect is further amplified by the relatively larger share of total demand associated with these segments (37% for EE and 36% for EI), compared to internal trips (27%). Hence the results show that disruptions affecting a limited number of strategic links translate into disproportionate network-wide impacts for these demand segments.

By contrast, vulnerability levels for the II segment are systematically lower. Internal trips are shorter on average (Table 7) and rely on a denser and more redundant urban road network, which provides a higher number of alternative paths. In this case, vulnerability emerges not from the disruption of high-capacity corridors, but from localized congestion effects on urban primary and secondary roads that already operate close to capacity under normal conditions.

The analysis of the top-ranked vulnerable links (Table 8 and Fig. 16) illustrates these mechanisms. For internal trips, critical links tend to correspond to urban roads supporting North–South and East–West paths, where flooding-induced rerouting concentrates traffic on links with limited residual capacity. For inter-ring and external trips, vulnerability instead concentrates on links that funnel traffic between the urban network, the ring road system, and the highway system, where flooding triggers major flows rerouting and severe congestion on infrastructure not designed to accommodate regional and national passing traffic.

Taken together with the network-level patterns reported in Fig. 16, these results suggest that flood-induced transport vulnerability is strongly shaped by the interaction between demand structure and functional road hierarchy. This implies that effective preparedness and mitigation strategies should be informed by differential impacts on demand segment: while internal-trip vulnerability may be addressed through localized traffic management and response measures aimed at facilitating flows and preserving residual capacity, vulnerability associated with inter-ring and external demand requires interventions on preserving functionality of strategic ring-road access points (e.g., via predictive dynamic traffic control, or temporary capacity management measures).

Fig. 18 assesses the sensitivity of the proposed vulnerability indicator to alternative assumptions on TR weighting. For each demand segment,

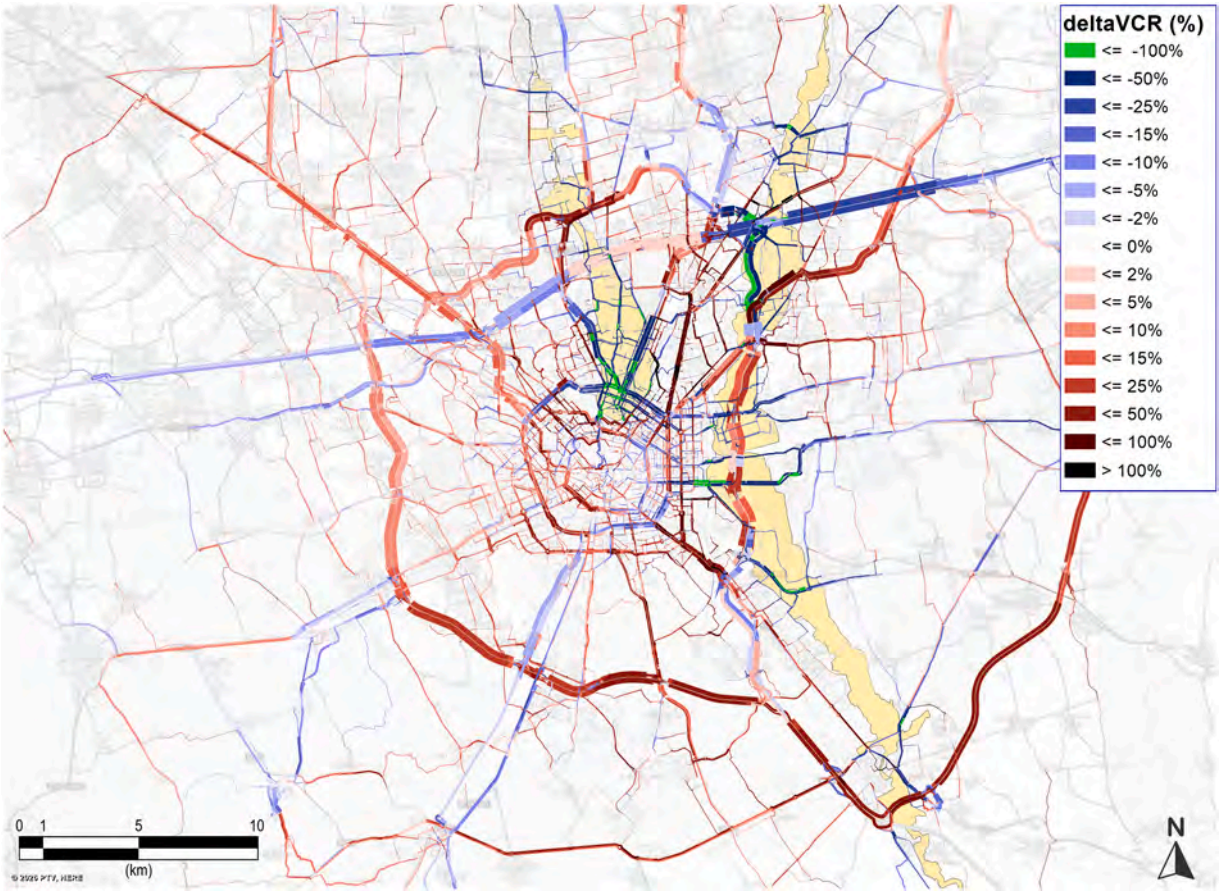

Fig. 14. Difference flow diagram for Flooding Scenario 5.

vulnerability rankings obtained are compared against rankings computed using uniform TR and capped TR (i.e. the TR of Sc4 and Sc5 is set to 500). Results show a very high rank correlation between the original and capped-TR one (Spearman's rank coefficient $\rho \approx 0.99$ across all demand segments), indicating that the identification of critical links is not driven by the most extreme events and that vulnerabilities arise mainly from the network's topology and demand patterns. When uniform TR weights are adopted, rank correlations decrease but remain substantial (ρ between 0.71 and 0.83), showing that scenario probabilities influence link prioritization without disrupting it. Importantly, the highest ranked links exhibit a high degree of stability across all the three TR weighing settings, suggesting that the proposed indicator provides robust prioritization of the most critical road links.

Fig. 19 compares the ranking of road links obtained with the composite vulnerability indicator (Eq. (6)) against a benchmark based solely on $\Delta VEHH$, as calculated in Eq. (2). As previously discussed in Section 3, $\Delta VEHH$ has been adapted in order to model the global relevance that a road link gains at the network level. Indeed, it represents the change in the change in vehicle-hours travelled of all the paths that utilize that link in the flood scenario, thereby representing the change in systemic relevance of a road link. Therefore, this metric does not represent the classic network-level indicator of impact of a link failure (as intended by Scott et al. (Scott, Novak, Aultman-Hall, and Guo, 2006)), but the exact opposite: the link-level indicator capturing the impact of a systemic, spatially distributed failure. Additionally, for the sake of benchmark comparison, $\Delta VEHH$ values were standardized and combined over scenarios using the same TR weighing system applied to the proposed vulnerability indicator.

The two rankings exhibit a substantial level of agreement (Spearman's rank coefficient $\rho = 0.80$), indicating that the proposed indicator remains consistent with a standard global performance-based metric.

At the same time, notable differences emerge among the rankings of the most critical links, which are identified as high priority by the composite indicator but ranked as less critical when considering $\Delta VEHH$ alone. These differences reflect the additional information captured by the composite indicator through the inclusion of the ΔVCR component, that represents congestion-related effects. Links characterized by high levels of saturation under flood conditions may generate severe local congestion without necessarily producing the largest increases in total path travel time of vehicles using that link. While such effects are only partially captured by $\Delta VEHH$, they are explicitly accounted for in the composite indicator, leading to a different prioritization of critical links.

These results suggest that, while $\Delta VEHH$ provides a valuable measure of global network performance degradation at the link-level, the proposed indicator offers a more informative representation of link criticality when the objective is to identify infrastructure elements that are prone to localized congestion and operational failure under flooding conditions and that should be a primary target of intervention.

Overall, the results highlight how flood-induced transport vulnerability emerges from the interaction between hazard exposure and probability, network structure, and demand composition, rather than from any single dimension alone. By combining local congestion effects and the global impact on traffic flows within a weighted multi-scenario framework, the proposed indicator allows for a differentiated identification of critical road links across demand segments. The application to the Milan case study shows that vulnerability varies substantially depending on the demand segment considered: while internal trips are primarily affected by localized (and pre-existing) congestion in the dense urban network, inter-ring and external trips are more sensitive to main corridors and related access points. These findings demonstrate the importance of adopting demand-segmented and systemic approaches when identifying priorities for transport preparedness and response to

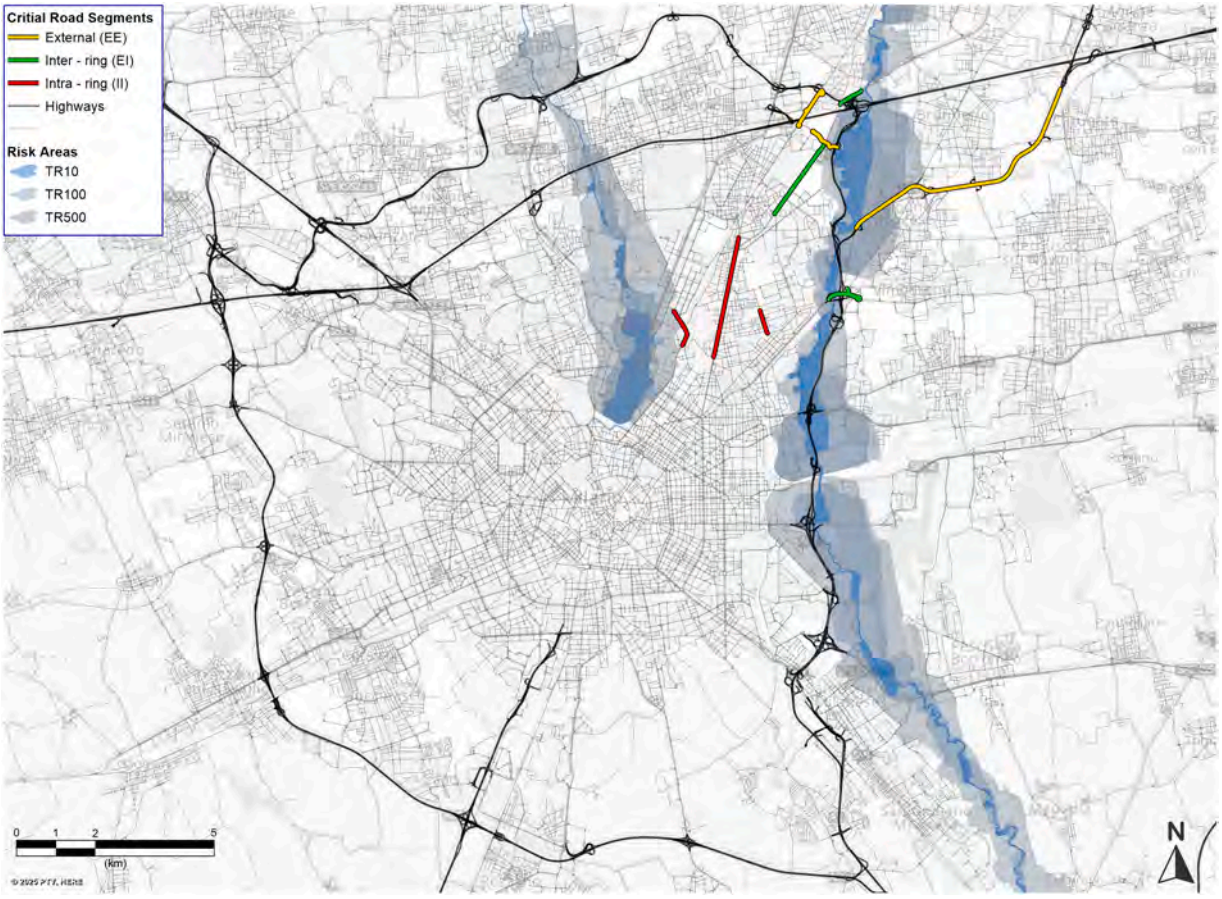

Fig. 15. Top 3 most critical road links by DAS (map).

Table 8
Top 3 most critical road links by DAS.

ID	DAS	Road Link	Vulnerability Value ($\times 10^{-3}$)
II_1	II	Via Emilio de Marchi (MI), western part	2.32
II_2	II	Viale Monza (MI), between Turro and Sesto Marelli	1.53
II_3	II	Via Ponte Nuovo (MI), southern part	1.35
EI_1	EI	Via Palmanova (MI), SP11 - A51 junction	49.22
EI_2	EI	Viale Italia (SSG), between viale Rimembranze and via Vulcano	25.82
EI_3	EI	Via Marconi (MZ), Monza junction	24.63
EE_1	EE	Viale Valtellina (CB)	51.05
EE_2	EE	A51, between Cologno Monzese and Agrate	46.57
EE_3	EE	Via Vulcano, A52 junction	36.39

the risk of flooding.

Finally, while the results are discussed with reference to the Milan case study, their transferability should be interpreted in relation to the interaction between road infrastructure and flood exposure patterns. Similar vulnerability mechanisms are expected in metropolitan contexts where flood-prone areas are located in proximity to ring-road systems or major radial corridors, such that disruptions affect key access points and induce large-scale traffic rerouting toward alternative, lower-capacity collector links. In this sense, the relevance of the findings does not rest solely on the representativeness of Milan's urban structure as a case study, but more fundamentally on the ability of the proposed methodology to highlight how demand composition, network structure, and hazard spatial patterns and variability jointly influence transport vulnerability. The framework therefore may provide transferable and policy-relevant insights for cities exhibiting comparable infrastructure and hazard configurations, while remaining adaptable to different urban forms and flood scenarios at the methodological level.

7. Conclusions

This study proposed a multi-scenario, demand-segmented framework to assess the vulnerability of urban road networks to flood-induced disruptions and applied it to the Milan metropolitan area. By integrating flood hazard information with a static traffic assignment model, the analysis shows that flood-related transport vulnerability does not arise solely from the inundation of specific road sections, but from the interaction between spatially distributed hazard impacts, network structure, and travel demand patterns.

Results indicate that major vulnerabilities concentrate along the ring-road systems and their radial access corridors, particularly in the proximity of flood-prone areas. Inter-ring and external trips are disproportionately affected, as disruptions along these corridors induce large-scale traffic rerouting and congestion spillovers onto lower-capacity links. In contrast, vulnerability for internal trips mainly reflects localized congestion effects within the dense urban network. These findings confirm that flood-related impacts are highly distributive and that demand heterogeneity is a key dimension of analysis in vulnerability assessment, that should be more commonly addressed.

Beyond the case study, the paper contributes methodologically to flood-related transport vulnerability assessment in three main ways. First, it explicitly addresses link-level systemic vulnerabilities of spatially diffused and probabilistic disruptions, by pinpointing localized criticalities, something that topological or accessibility analyses fail either in capturing the supply-demand interaction of or in identifying the critical components. Second, it introduces a composite link-level

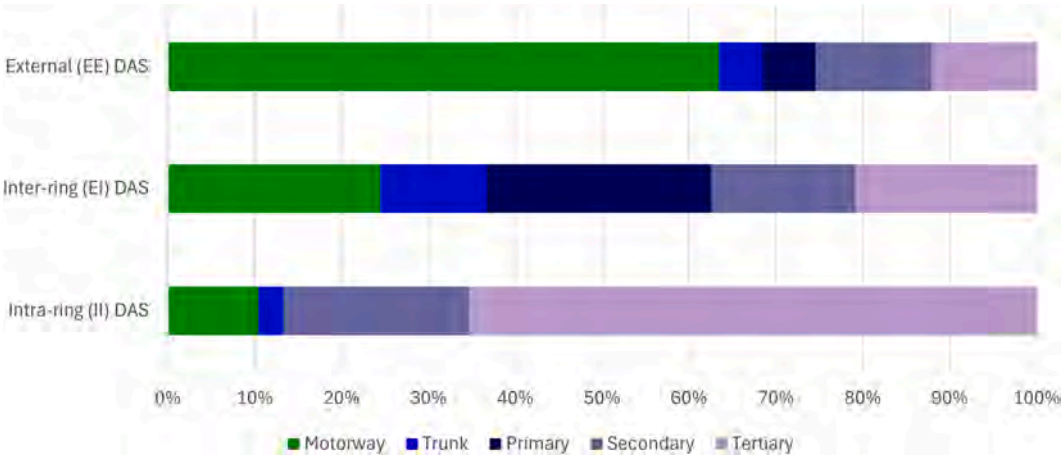

Fig. 16. Link type incidence by share of total length, for the top 100 most vulnerable links by DAS.

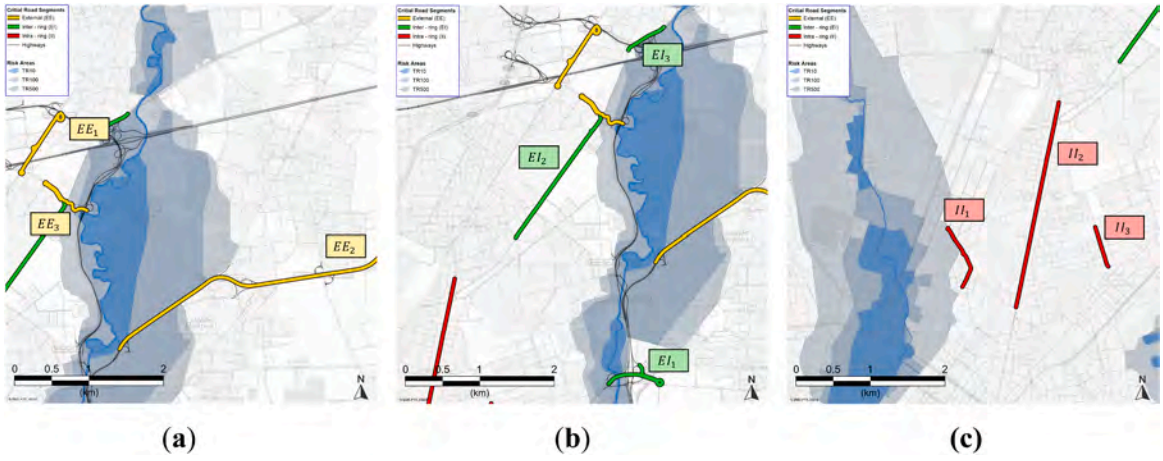

Fig. 17. Close Up - Most critical road links per DASs. (a) EE segment. (b) EI segment. (c) II segment.

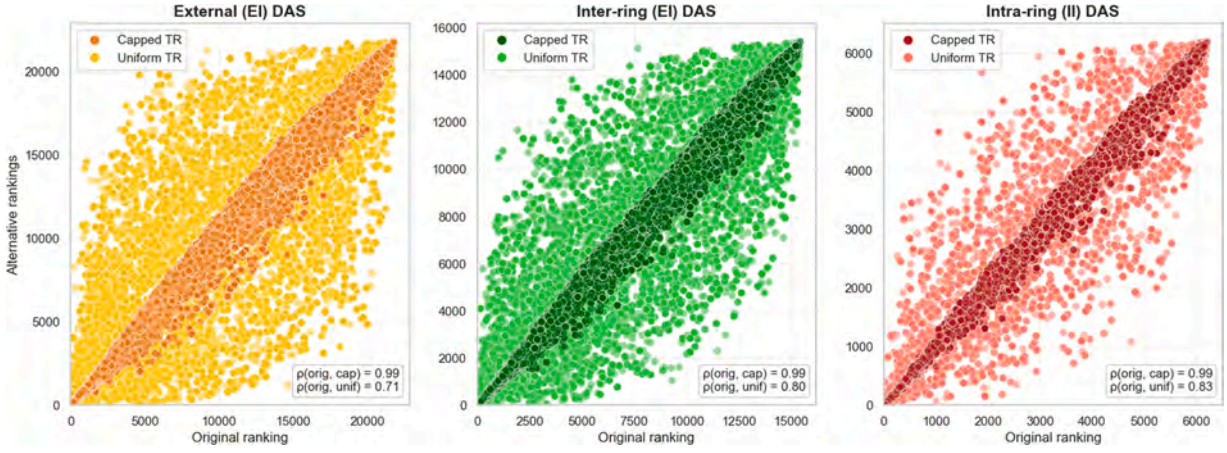

Fig. 18. Sensitivity analysis of the vulnerability ranking obtained with the proposed indicator to alternative TR weighing settings per demand segment. The lower the rank number, the higher the vulnerability score.

vulnerability indicator that combines local congestion effects with the systemic relevance of road links under disruption, allowing the identification of links that become critical because they absorb network-wide stress. Third, demand segmentation is treated as a core analytical dimension, demonstrating that vulnerability patterns and criticality rankings differ substantially across travel segments and that aggregate analyses may unintentionally discard more targeted policy-relevant insights.

From a policy-making perspective, the proposed framework is best interpreted as a decision-support tool for preparedness and prioritization under uncertainty. Its primary value lies in identifying, *ex ante*, which road segments are most likely to become critical under plausible

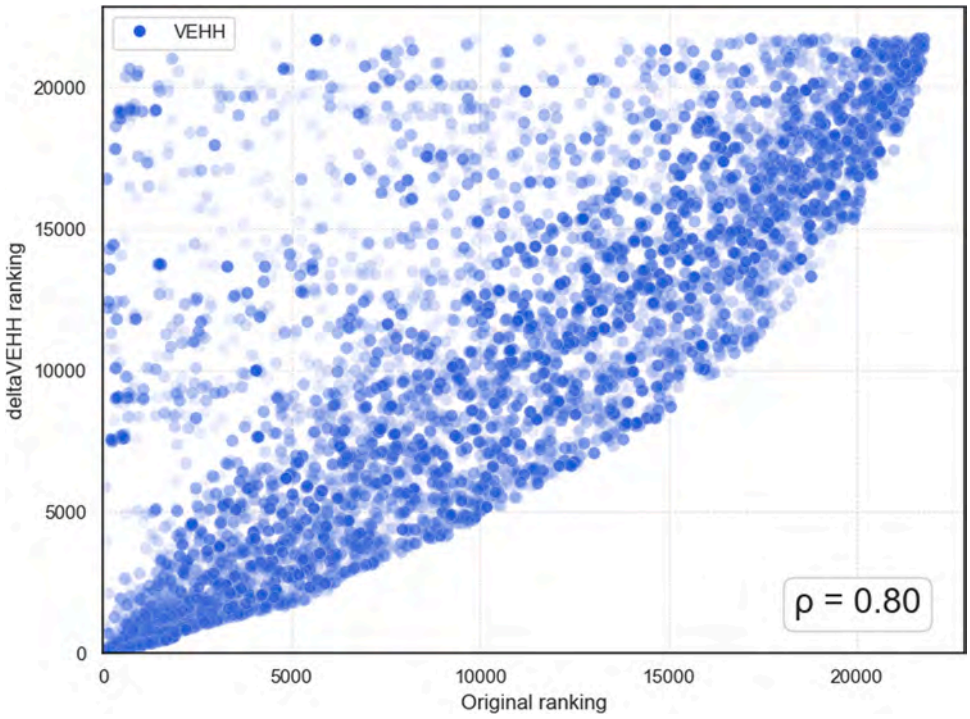

Fig. 19. Benchmark comparison between the vulnerability ranking obtained with the proposed indicator (Eq. (6)) and a $\Delta VEHH$ ranking. The lower the rank number, the higher the vulnerability score.

flood scenarios and for which demand segments. This supports targeted preparedness strategies, such as preserving minimum functional capacity along key ring-road access points, implementing temporary capacity management or predefined traffic rerouting schemes, and prioritizing interventions where disruptions are expected to generate disproportionate system-wide impacts. Structural flood mitigation measures, such as detention basins or flood barriers, may also yield significant indirect transport benefits when they reduce the frequency or severity of flood scenarios affecting these vulnerable points. Additionally, the results point out the relevance of coordinating risk management with land-use regulation and public transport planning, as both can be valuable tools for reducing flood-related transport risk. In fact, land use policy can contribute to mitigating risk by preventing car mobility demand from concentrating into flood-prone areas (e.g., by preventing residential sprawl or surface-intensive industrial and commercial development). Promoting sustainable alternatives to car transport (e.g., public transport and bicycle infrastructure) can also promote robustness by calming or diverting demand for private transport in the event of flooding.

While the findings are discussed with reference to the case study of Milan, their transferability can be accounted for in two ways. First, Milan features a common urban structure characterized by a radial-ring road structure, with flood-prone corridors that coincide with key access points. Similar vulnerability patterns may be expected in cities where flooding affects ring-road systems or major radial connections, inducing large-scale rerouting toward lower-capacity alternatives. Second, while the specific ranking of critical links is case-dependent, the vulnerability assessment methodology and the analytical foundation underpinning are easily transferable to other urban contexts where macroscopic models and flood risk areas are available.

Several limitations should be acknowledged. Both the hazard and the transport system are represented statically: flood and traffic temporal dynamics are not modelled; thus, the analysis focuses on immediate performance degradation rather than recovery or long-term resilience. The transport model is monomodal and demand is treated as fixed, without accounting for trip cancellations or behavioural adaptation. Flood depths are represented through discrete assumed values rather than detailed hydraulic modelling, and the macroscopic traffic model does not capture limited user knowledge or more detailed vehicle interactions to be expected under flooded conditions. Despite said constraints in behavioural realism, these simplifications are consistent with the goal of supporting the identification of interventions and the targeted design of preparedness and mitigation policies.

Future research could extend this framework toward a more comprehensive resilience analysis by integrating dynamic flood propagation, dynamic traffic assignment, and agent-based or microsimulation approaches. Incorporating endogenous demand responses and multimodal interactions would further enhance the representation of system behaviour under flooding. Additionally, other demand segmentation criteria may be considered (i.e., socioeconomic, by trip purpose, by transport mode, etc.) to reveal different vulnerability patterns. In this perspective, the proposed framework provides an effective screening and prioritization tool that can be further enhanced.

CRediT authorship contribution statement

Francesco Guglielmi: Writing – review & editing, Writing – original draft, Visualization, Software, Resources, Methodology, Formal analysis, Data curation, Conceptualization. **Pietro Mariano:** Writing – review & editing, Writing – original draft, Visualization, Software, Resources, Methodology, Formal analysis, Data curation, Conceptualization. **Pierluigi Coppola:** Validation, Supervision, Methodology, Conceptualization.

Declaration of competing interest

The authors declare that they have no known competing financial interests or personal relationships that could have appeared to influence the work reported in this paper.

References

ITF. (2016). Adapting transport to climate change and extreme weather. *ITF research reports*. OECD. ISBN 9789282108062.

ITF. (2024). *Transport system resilience: Summary and conclusions*. OECD. ISBN 978-92-821-1692-0.

Coppola, P., & Esztergár-Kiss, D. (Eds.). (2019). *Autonomous vehicles and future mobility*. Elsevier. ISBN 9780128176962.

Bruneau, M., Chang, S. E., Eguchi, R. T., Lee, G. C., O'Rourke, T. D., Reinhorn, A. M., Shinozuka, M., Tierney, K., Wallace, W. A., & Von Winterfeldt, D. (2003). A framework to quantitatively assess and enhance the seismic resilience of communities. *Earthquake Spectra, 19*, 733–752. https://doi.org/10.1193/1.1623497

McDaniels, T., Chang, S., Cole, D., Mikawoz, J., & Longstaff, H. (2008). Fostering resilience to extreme events within infrastructure systems: Characterizing decision contexts for mitigation and adaptation. *Global Environmental Change, 18*, 310–318. https://doi.org/10.1016/j.gloenvcha.2008.03.001

Bešinović, N. (2020). Resilience in railway transport systems: A literature review and research agenda. *Transp. Rev., 40*, 457–478. https://doi.org/10.1080/01441647.2020.1728419

Gonçalves, L. A. P. J., & Ribeiro, P. J. G. (2020). Resilience of Urban transportation systems. Concept, characteristics, and methods. *J. Transp. Geogr., 85*, Article 102727. https://doi.org/10.1016/j.jtrangeo.2020.102727

Berdica, K. (2002). An introduction to road vulnerability: What has been done, is done and should Be done. *Transp. Policy (Oxf), 9*, 117–127. https://doi.org/10.1016/S0967-070X(02)00011-2

Comune di Milano La vasca di laminazione delle piene del seveso Available online: https://www.comune.milano.it/argomenti/ambiente-e-animali/la-vasca-di-laminazione-delle-piene-del-seveso (accessed on 30 June 2026).

Comune di Milano *Piano aria e clima*.

Comune di Milano *Piano di governo del territorio (PGT)*.

Mattsson, L.-G., & Jenelius, E. (2015). Vulnerability and resilience of transport systems – A discussion of recent research. *Transp. Res. Part A Policy Pract., 81*, 16–34. https://doi.org/10.1016/j.tra.2015.06.002

Jafino, B. A., Kwakkel, J., & Verbraeck, A. (2020). Transport network criticality metrics: A comparative analysis and a guideline for selection. *Transp. Rev., 40*, 241–264. https://doi.org/10.1080/01441647.2019.1703843

Zhou, Y., Wang, J., & Yang, H. (2019). Resilience of transportation systems: Concepts and comprehensive review. *IEEE Transactions on Intelligent Transportation Systems, 20*, 4262–4276. https://doi.org/10.1109/TITS.2018.2883766

Sun, W., Bocchini, P., & Davison, B. D. (2020). Resilience metrics and measurement methods for transportation infrastructure: The State of the art. *Sustain. Resilient Infrastruct, 5*, 168–199.

Almotahari, A., & Yazici, A. (2020). Impact of topology and congestion on link criticality rankings in transportation networks. *Transp. Res. D Transp. Environ., 87*, Article 102529. https://doi.org/10.1016/j.trd.2020.102529

Chen, X.-Z., Lu, Q.-C., Peng, Z.-R., & Ash, J. E. (2015). Analysis of transportation network vulnerability under flooding disasters. *Transp. Res. Rec., 2532*, 37–44. https://doi.org/10.3141/2532-05

Shen, S., & Kim, K. (2020). Assessment of transportation system vulnerabilities to tidal flooding in Honolulu, Hawaii. *Transp. Res. Rec., 2674*, 207–219. https://doi.org/10.1177/0361198120940680

Pregnolato, M., Ford, A., Wilkinson, S. M., & Dawson, R. J. (2017). The impact of flooding on road transport: A depth-disruption function. *Transp. Res. D Transp. Environ., 55*, 67–81. https://doi.org/10.1016/j.trd.2017.06.020

Pregnolato, M., Ford, A., Robson, C., Glenis, V., Barr, S., & Dawson, R. (2016). Assessing urban strategies for reducing the impacts of extreme weather on infrastructure networks. *R. Soc. Open Sci., 3*, Article 160023. https://doi.org/10.1098/rsos.160023

Papilloud, T., & Keiler, M. (2021). Vulnerability patterns of road network to extreme floods based on accessibility measures. *Transp. Res. D Transp. Environ., 100*, Article 103045. https://doi.org/10.1016/j.trd.2021.103045

Loreti, S., Ser-Giacomi, E., Zischg, A., Keiler, M., & Barthelemy, M. (2022). Local impacts on road networks and access to critical locations during extreme floods. *Sci. Rep., 12*, 1552. https://doi.org/10.1038/s41598-022-04927-3

Abdulla, B., Kiaghadi, A., Rifai, H. S., & Birgisson, B. (2020). Characterization of vulnerability of road networks to fluvial flooding using SIS network diffusion model. *Journal of Infrastructure Preservation and Resilience, 1*, 6. https://doi.org/10.1186/s43065-020-00004-z

Marian, A. R., Hijazi, R., Masad, E., & Abdel-Wahab, A. (2024). Quantifying the vulnerability of road networks to flood-induced closures using traffic simulation. *Transportation Engineering, 17*, Article 100262. https://doi.org/10.1016/j.treng.2024.100262

Borowska-Stefańska, M., Bartnik, A., Goniewicz, K., Kowalski, M., Sahebgharani, A., Tomalski, P., & Wiśniewski, S. (2025). Assessing road network resilience and vulnerability in urban transport systems against Urban flooding. *Environmental Hazards*, 1–24. https://doi.org/10.1080/17477891.2025.2469634

Borowska-Stefańska, M., Bartnik, A., Dulebenets, M. A., Kowalski, M., Sahebgharani, A., Tomalski, P., & Wiśniewski, S. (2024). Changes in intra-City transport accessibility accompanying the occurrence of an urban flood. *Transp. Res. D Transp. Environ., 126*, Article 104040. https://doi.org/10.1016/j.trd.2023.104040

Dong, S., Gao, X., Mostafavi, A., & Gao, J. (2022). Modest flooding can trigger catastrophic road network collapse due to compound failure. *Commun. Earth Environ., 3*, 38. https://doi.org/10.1038/s43247-022-00366-0

Lin, X., Lu, Q., Chen, L., & Brilakis, I. (2024). Assessing dynamic congestion risks of flood-disrupted transportation network systems through time-variant topological analysis and traffic demand dynamics. *Advanced Engineering Informatics, 62*, Article 102672. https://doi.org/10.1016/j.aei.2024.102672

Dowds, J., Sentoff, K., Sullivan, J. L., & Aultman-Hall, L. (2017). Impacts of model resolution on transportation network criticality rankings. *Transp. Res. Rec., 2653*, 93–100. https://doi.org/10.3141/2653-11

Tsang, M., & Scott, D. M. (2020). An integrated approach to modeling the impact of floods on emergency services: A case study of Calgary, Alberta. *J. Transp. Geogr.*, 86. https://doi.org/10.1016/j.jtrangeo.2020.102774

Crosson, C., Tong, D., & Zhang, Y. (2020). *Urban transportation system flood vulnerability assessment with special reference to low income and minority neighborhoods*. Transportation Research and Education Center (TREC).

Pagliara, F., & Zingone, M. (2023). Providing resilience due to adverse weather events: A cost-benefit analysis for the case of the Milan Malpensa Airport in Italy. *J. Air Transp. Manag., 113*, Article 102484. https://doi.org/10.1016/j.jairtraman.2023.102484

Lyman, K., & Bertini, R. L. (2008). Using travel time reliability measures to improve regional transportation planning and operations. *Transp. Res. Rec.*, 1–10. https://doi.org/10.3141/2046-01

Scott, D., Novak, D., Aultman-Hall, L., & Guo, F. (2006). Network robustness Index: A new method for identifying critical links and evaluating the performance of transportation networks. *J. Transp. Geogr., 14*, 215–227. https://doi.org/10.1016/j.jtrangeo.2005.10.003

Highway capacity manual (7th Edition). (2022). Washington, D.C.: National Academies Press. ISBN 978-0-309-27566-8.

Cascetta, E. (2009). *Transportation systems analysis, 29*. Boston, MA: Springer US. ISBN 978-0-387-75856-5.

Autorità di Bacino Disrettuale del Fiume Po (ADBPO) *Aggiornamento e revisione Delle Mappe Dipericolosità e Del Rischio Di Alluvione redatte Aisensi Dell'art. 6 Del D.Lgs. 49/2010 Attuativodella dir. 2007/60/CE – II Ciclo Di Gestione - Relazione Metodologica*; 2020.

Rose, J. G., & Gallaway, B. M. (1977). Water depth influence on pavement friction. *Transportation Engineering Journal of ASCE, 103*, 491–506. https://doi.org/10.1061/TPEJAN.0000648

Cerezo, V., & Gothié, M. (2009). Adhera research: A new approach for pavement performance evaluation. *Wear : an international journal on the science and technology of friction lubrication and wear, 267*, 1105–1110. https://doi.org/10.1016/j.wear.2009.02.022

Al-Qadami, E. H. H., Mustaffa, Z., Al-Atroush, M. E., Martinez-Gomariz, E., Teo, F. Y., & El-Husseini, Y. (2022). A numerical approach to understand the responses of passenger vehicles moving through floodwaters. *J. Flood Risk Manag., 15*. https://doi.org/10.1111/jfr3.12828